DOI: https://doi.org/10.24297/jap.v24i.9872

Prototyping of self-sustaining propulsion systems for solar system exploration

Ramon Ferreiro Garcia

Former Prof. Emeritus at the Industrial Eng. Dept., University of A Coruna Spain

Abstract

This work aims at acquiring deeper knowledge about solar system components including valuable materials as well as clearing viable ways towards extra solar systems. To achieve as much as possible the proposed objectives a viable Self-Sustaining Power Machine (SSPM), including an energy supply and propulsion paradigm shift is proposed. This system will replace the Nuclear Thermal Power and Nuclear Electric Propulsion Systems avoiding its inherent drawbacks, constraints and limitations. Therefore, this research addresses the need to firstly explore accessible celestial bodies within our solar system—planets, their moons and valuable accessible asteroids to utilize their resources.

A primary challenge in this endeavor is ensuring a reliable energy supply. Consequently, this article proposes a disruptive change in both: energy supply and propulsion technology, replacing nuclear-based systems with SSPMs. These autonomous space vehicles would integrate the necessary SSPM-based resources to supply electrical power to all critical services and/or systems.

Research results indicate us that the propellant fluid is crucial for achieving optimal results (high specific heat and low density with a high adiabatic expansion coefficient) —(H_2). High temperature allows for high propellant expulsion velocity, resulting in high specific impulse and high thrust under lower propellant flow rate. Hydrogen (H_2) dramatically outperforms Nitrogen (N_2). At 3000K, H_2 achieves an exhaust velocity of 10.34 km/s (Isp ~1054 s), while N_2 only reaches 2.74 km/s (Isp ~280 s). H_2 produces significantly more thrust than N_2 under the same conditions. For example, at a mass flow rate of 100 kg/s and 3000K, H_2 generates ~103.4 tons of thrust, while N_2 generates only ~27.4 tons (Tables 17 & 20). With 50 tons of propellant to push a 10-ton spacecraft, H_2 heated to 3000K can achieve a final velocity of ~26.5 km/s. N_2 under the same conditions can only reach ~7.0 km/s, a massive difference in transit time and mission reach

Keywords: Self-Sustaining Power Generation, Cascaded Coupled Power Units, Constant Temperature Drop, Vacuum-Induced useful work, Thermodynamic Disruption.

Nomenclature related to general sVsVs cycles and SSPG	
Acronyms	**Description/Context**
Cont, cont	Subscript of contraction process: A form of compression (volume decrease) achieved by cooling a TWF, which generates a **pull** force while increasing internal energy and pressure.
CTF	Cooling Transfer Fluid (conventionally, thermal oil)
E_i	Energy input (heat and/or work)
EM	Electromagnetic
E_o	Energy output (heat and/or work)
EP	Electric Power
TEP	Total real or effective electric power (the effective generator output power)
NEP	Net electric power: NEP=TEP-qi_feedback (available useful EP)
Exp, exp.	Subscript of expansion process: A form of expansion (volume increase) achieved by heating a TWF, which generates a **push** force while decreasing internal energy and pressure.
FCF	Forced convection fan (recirculation fan of the TWF)
FP	Feed pump (feed compressor of the TWF)
Gen	Electric Power Generator: alternator or generator
H, L	Subscript of High, Low: i.e. T_L with L subscript of T_{low}, T_H, with H subscript of T_{high}
HTF	Heating Transfer Fluid (conventionally, liquid as thermal oil or gas as H_2)
Is_eff	Isentropic efficiency: (open processes). losses factor inherent to real gas exp/comp.
LF	Losses factor (include thermo-mechanical and thermo-hydraulic losses)
PU	Power Unit driven by the thermal cycle sVsVs or VsVs cycle
qi_feedback(PU1	Electric power as heat added to the first cascaded PU. qi_elect_PU1 = (h_2-h_1) of PU1
RF	Heat recovery factor (heat transfer losses including heat leaks)
sp	State point of any stationary point state of a thermal cycle
SSPM	Self-Sustaining Power Machine, Self-Sufficient Power Machine
SSPG	Self-Sustaining Power Generator, Self-Sufficient Power Generator

Suct, suct.	Subscript of suction process: A form of expansion (volume increase) achieved by adding useful work to the system by means of a **pull** force, while decreasing internal energy and pressure.
TWF	Thermal Working fluid (a gas with high adiabatic expansion coefficient such as helium or argon..)
sVsVs	sequential processes: Isentropic **s**, Isochoric **V**, adiabatic **s**, Isochoric **V**, adiabatic **s**: [s**VsVs**]
TF (%)	Heat transfer losses due t heat recovery effectiveness
LF (%)	Losses factor (thermal and mechanical irreversibilities)
η_{th} (%)	Cycle thermal efficiency [w_n/qi]
Symbols/units	***description***
p(bar)	pressure
q_i(kJ/kg)	specific heat in to a cycle process
q_{i23} (kJ/kg)	Input heat to cycle process 2-3
q_o(kJ/kg)	specific heat out from a cycle process
q_{o4-5} (kJ/kg)	output heat from cycle process 4-5 in a sVsVs cycle
q_{rec}	Recovered heat from cycle process 4-5 in every sVsVs cycle-based PU
Cp(kJ/kg-K)	specific heat capacity at constant pressure
Cv(kJ/kg-K)	specific heat capacity at constant volume
s(kJ/kg-K)	specific entropy
h(kJ/kg)	specific enthalpy; h=Cp.T; T=f(T)
T(K)	Absolute temperature
T_H(K)	top cycle temperature
T_L(K)	bottoming cycle temperature
u(kJ/kg)	specific internal energy
v(m^3/kg)	specific volume
V(m^3)	volume
w(kJ/kg)	specific work
w_i(kJ/kg)	specific work input
$w_{i12} = w_{iFP}$	Input work to the Feed Pump: $w_{iFP} = \Delta h_{12} = h_2 - h_1 = Cp \cdot (T_2 - T_1)$
w_o(kJ/kg)	specific work out
w_{oexp} (kJ/kg)	Output expansion work due to previously added heat
w_{ocont} (kJ/kg)	Output contraction work due to previously extracted heat
w_{oexp34} (kJ/kg)	Output expansion work w_{o34} due to previously added heat
$w_{ocont51}$ (kJ/kg)	Output contraction work w_{o51} due to previously extracted heat
w_n (kJ/kg)	Net useful work (w_{oexp} + w_{ocont}) = (w_{o34} + w_{o51}) in an VsVs thermal cycle
q_{rec}/PUi(kJ/kg	Heat recovered from every PU from cooling cycles processes
η_{th} (%)	Cycle thermal efficiency (w_n/qi)

Introduction

1.1 General perspective and context

The most important incentive to tackle complex tasks that require both the acquisition of knowledge related to the cosmic environment —and particularly the solar system— and, especially, the exploitation of valuable resources justifies this research. The context of the article is focused on the dawn of a space-based economy reliant on extracting water ice, volatiles, and metals from asteroids, solar system accessible planets and satellites including particularly the Moon and Mars. While high-thrust nuclear thermal propulsion (NTP) has long been the leading candidate for rapid crewed transport, nuclear electric propulsion (NEP) presents a viable alternative. Both systems, however, face significant hurdles—including fissile material availability, testing bans, public acceptance, and limited operational lifespan, which contribute to increment the final costs.

1.2 Identification of Critical Challenges

The greatest challenge concerning the exploitation of resources from our nearest cosmic environment—the solar system—lies in transportation. Conventional energy and propulsion techniques require the use of non-recoverable and therefore exhaustible materials—hydrogen and some noble gases, among others—which hinders the transport of propellant loads and considerably limits operational range. Therefore, the cost, time, and capability of propulsion are the fundamental limiters.

1.3 Current State-of-the-Art and Its Gaps

It is worth analyzing how high-thrust, high-specific-impulse nuclear thermal propulsion (NTP) has been the leading candidate for rapid crewed transport. However, nuclear electric propulsion (NEP) also has its disadvantages. Both, nevertheless, present challenges such as (e.g., availability of fissile material, testing bans, public acceptance, and short lifespan). To delve a little deeper into this topic let's explore What is the state of the art technologies dealing with inter-planetary nuclear propulsion.

The state of the art in interplanetary nuclear propulsion is experiencing a significant renaissance, moving from decades of theoretical studies and ground tests into active technology development and flight demonstration programs. It's no longer just a paper concept. Here is a breakdown of the two main categories, their current state, and key programs:

a) Nuclear Thermal Propulsion **(NTP**)

Concept: Uses a fission reactor to directly heat a propellant (typically liquid hydrogen) which then expands through a nozzle to produce thrust. Offers a compelling blend of high thrust (for shorter transit times) and moderately high specific impulse (Isp ~900 sec, about 2x that of chemical rockets).

State of the Art & Recent Advances: Propellant Element Development: This is the core challenge. Modern programs use Low-Enriched Uranium (LEU, <20% U-235) instead of the historical Highly Enriched Uranium (HEU) for non-proliferation and security reasons.

NASA/DRACO Program: The Demonstration Rocket for Agile Cislunar Operations (DRACO) was the flagship program as a research reference [1].

A partnership between NASA and DARPA, with Blue Origin and Lockheed Martin competing on the spacecraft design. It aims for an in-space flight test of an LEU-based NTP system in the late 2020s/early 2030s**.** This is the current cutting edge in practical development.

Propellant Materials: Research focuses on advanced carbide-based propellants (e.g., Uranium Zirconium Carbide, U-Zr-C) and ceramic-metallic (cermet) propellants, encapsulated in protective coatings to withstand extreme temperatures and hydrogen corrosion.

Testing: Extensive historical ground tests from projects like NERVA and Rover proved basic feasibility. Today advanced non-nuclear testing of components (injectors, nozzles, and turbopumps) and "nuclear-informed" testing of propellant elements in simulated environments is ongoing.

Key Advantage for Human Mars Missions: NTP can potentially reduce Mars transit time from 6-9 months (chemical) to ~4-5 months, drastically reducing crew exposure to cosmic radiation and microgravity.

b) Nuclear Electric Propulsion **(NEP)**

Concept: Uses a fission reactor to generate electricity (in the 100 kWe to MWe range), which then powers an electric thruster (like Hall-effect or ion thrusters) [2-4].

Power Conversion: The major challenge is creating lightweight, efficient, and reliable systems to convert reactor heat to electricity using conventional techniques such as:

Brayton Cycle (Gas Turbine): Currently the leading candidate for high-power systems (MWe), offering good efficiency and a path to scalability.

Stirling Cycle: Being researched for lower-power systems, offering high efficiency at smaller scales.

Reactor Design: Projects like NASA's Fission Surface Power project [5] for lunar bases are directly relevant.

They are developing compact, 40-kWe class uranium fission reactors with passive safety for in-space use.

Scaling this to the 100s of kWe or MWe needed for fast interplanetary NEP is the next step.

Radiator Technology: A critical and often overlooked subsystem. Rejecting waste heat in space requires massive, lightweight radiators. Advanced composite materials and liquid droplet radiator concepts are being studied to reduce radiator mass. To reduce radiator mass for interplanetary transit, researchers are exploring advanced composites like carbon-polymer or carbon-carbon (C-C) for lightweight, high-conductivity panels, and explore Liquid Droplet Radiators (LDRs) that use streams of liquid droplets (like silicone oils or liquid metals) to radiate heat, offering lower specific mass and compact stowage compared to traditional rigid panels.

1.3.1 Advanced Composite Materials

a) Carbon-Polymer/Carbon-Carbon (C-C) Composites: These are favored over aluminum due to lower density, high thermal conductivity, and low thermal expansion, drastically reducing radiator weight.

b) Pyrolytic Graphite Sheets (PGS): Encapsulated within composites, these offer exceptional thermal conductivity, creating lighter, more efficient heat rejection surfaces.

c) Nanoparticle-Enhanced Composites: Adding materials like graphene, carbon nanotubes, or silica nanoparticles to polymer matrices further boosts thermal performance and strength.

1.3.2 Liquid Droplet Radiator (LDR) Concepts

How it Works: An LDR sprays a fluid (like liquid metal or silicone oil) into a stream of droplets that radiate heat into space before being collected and recirculated, acting as a vast, deployable radiator.

a) Coolant Options:

Low Temp (250-350 K): Silicone oils, siloxanes (e.g., Trimethyl-Pentaphenyl-Trisiloxane).

Mid-High Temp (370-650 K): Liquid metal eutectics.

b) High Temp (500-1000 K): liquid tin.

Advantages: LDRs can be stowed compactly, are easier to deploy, and have a lower specific mass (mass per unit area) than traditional radiators, making them ideal for high-power missions.

c) Electric Thrusters: While ion and Hall thrusters are flight-proven (e.g., on satellites and missions like Dawn), scaling them up to the 100s of kW or MW power levels needed for crewed NEP is an active area of research [6] (e.g., magnetoplasmadynamic (MPD) thrusters, high-power Hall thrusters [2]).

1.3.3 Cutting-Edge Concepts & Programs

Bimodal NTP/NEP: Systems that can operate in both modes—using the reactor for high-thrust NTP during major maneuvers and for high-efficiency NEP for orbital adjustments or powering ship systems. This is a leading concept for flexible mission architectures.

NASA's Nuclear Evolutionary Concept (NEX) Studies: Ongoing system-level studies exploring various reactor, power conversion [7], and thruster combinations for future crewed missions to Mars and beyond. For more information see [8-10] NASA's Kilopower Reactor Development and the Path to Higher Power Missions.

Advanced Propellants & Materials: Research into novel propellants, claddings, and moderators that allow for higher operating temperatures (improving Isp and efficiency) and longer life.

Major Challenges & Focal Points of Current R&D:

Materials Science: Propellant elements that can withstand >2700K temperatures without corroding in hot hydrogen (for NTP). Reactor and radiator materials for long-duration NEP (10+ years).

System Integration & Mass: The "mass penalty" of the reactor, shielding, and power conversion/radiators must be offset by the performance gains. Minimizing system mass is paramount.

Safety & Public Acceptance: Ensuring safety during launch (accident scenarios) and in-space operation. The use of LEU helps here. Clear communication of safety protocols is critical.

In-Space Testing: Programs like DRACO are vital to move from ground tests to a validated in-space technology. There is no full-scale test facility on Earth that can test an operating NTP engine firing into a vacuum.

To conclude, the state of the art is highly active and promising. **NTP** is closer to a near-term flight demonstration (DRACO cancelled in June, 2025), focused on rapid human transit. **NEP** is further out on the timeline but is essential for extremely efficient, high-capacity cargo missions and future robotic exploration of the outer solar system.

1.3.4 Key Advantages

High Efficiency: Achieves a high specific impulse (propellant escape velocity). Abundant Power: Generates a large amount of electricity for the spacecraft and science, unlike limited solar power.

Faster Missions: Enables shorter transit times to destinations such as Mars or the Saturn system [9].

Lower Propellant Mass: Drastically reduces the need for heavy chemical propellant.

Solar Independence: Requires no sunlight, operating anywhere in the solar system.

Applications: Exploration of the outer solar system.

Crewed missions to Mars, offering faster round trips.

Maintenance of space stations such as the future Lunar Gateway.

Current Status: Key components (reactors, power systems) are being developed and tested to bring NEP technology to the Technology Readiness Levels (TRLs) required for future missions, with plans for power systems ranging from hundreds of kilowatts to megawatts.

1.4 Main drawbacks Inherent to NTP and NEP reactors

Despite the remarkable advances related to safety in nuclear systems, certain problems exist that are difficult or impossible to solve. The main drawbacks of nuclear reactors for space propulsion are safety/radiation risks (catastrophic fallout on launch failure, crew/instrument exposure), weight (heavy shielding, reactor core), technical complexity (extreme heat management in vacuum, slow start/stop, radioactive waste), **cost**, and public/political hurdles, making them unsuitable for Earth launch but viable for deep space missions where their high efficiency outweighs risks and weight penalties.

Safety & Environmental Concerns

Launch Hazard: A launch failure could spread highly radioactive materials globally, making ground launches extremely risky and generally prohibited.

Crew/Payload Radiation: Requires heavy shielding, adding significant mass, to protect astronauts and sensitive instruments from reactor radiation.

Radioactive Waste: Generates radioactive byproducts that need complex management in space.

Engineering & Operational Challenges

Extreme Heat: Reactors produce immense heat, requiring complex radiators for cooling in the vacuum of space, as they can't rely on water cooling like on Earth.

a) Weight: The reactor core, shielding, and cooling systems add substantial mass, impacting payload capacity.

b) Control Complexity: Managing reactor startup, shutdown, and heat dissipation in microgravity is technically challenging; running out of propellant can lead to core meltdown.

c) Radioactive Operation: Becomes highly radioactive during use, complicating testing and maintenance.

Cost & Politics

High Cost: Development, propellant (uranium/plutonium), and specialized facilities are very expensive.

Public & Political Opposition: Stigma, safety fears, and ethical concerns hinder widespread adoption.

Suitability

a) Not for Earth Launch: Unsuitable for initial liftoff from Earth due to fallout risks.

b) Best for Deep Space: Ideal for interplanetary missions where high performance (specific impulse) justifies the weight and risks, often assembled in orbit.

1.5 Heat-based techniques for supplying power and propulsion thrust

Propulsive efficiency in space is a function of propellant temperature. Hence, the relevance and necessity of achieving high propellant temperatures before expansion in the propulsion nozzle. Likewise, high pressure, achieved at low cost through compression of the liquid propellant, enhances the efficiency of the propulsion system, as well as that of self-sufficient electric generators. For these reasons, this introduction also includes concepts related to heating the propellant at temperatures limited only by the materials of both the propulsion systems and the self-sufficient generators. However, for spacecraft services equipped with Self-Sustaining Power Machines (SSPMs) which includes al services power and propulsion, the maximum required temperatures is lower than 10000 K.

1.5.1 High temperature-based heat transfer tecniques

Heating gases to extreme temperatures (from thousands to millions of degrees Kelvin) is a critical challenge in fields like aerospace, fusion energy, and advanced materials. The most advanced techniques leverage electromagnetic energy to transfer heat directly, precisely, or volumetrically, avoiding material limits of traditional conductive heaters. Here's a breakdown of the most advanced techniques, categorized by energy source:

1.5.2 Laser-Based Heating

Lasers provide extreme power density, precise spatial/temporal control, and can heat a target without physical contact.

Mechanism: Photons are absorbed by the gas molecules/atoms or a solid target (which then heats the gas), leading to rapid heating, dissociation, and ionization.

Advanced Techniques:

a Laser-Driven Plasma Heating (Inertial Confinement Fusion - ICF): The world's most powerful lasers (e.g., the NIF in the US) fire multiple beams simultaneously onto a millimetre-sized propellant capsule containing deuterium-tritium gas. The intense laser radiation (in the form of X-rays, generated within a hohlraum) destroys the outer layer, imploding the propellant at densities and temperatures (~100 million °C) sufficient for nuclear fusion.

b Laser Sustained Plasmas (LSP): A high-power continuous-wave or pulsed laser (e.g., CO_2, diode) is focused into a gas chamber. The laser ionizes a seed of gas, creating a small plasma that strongly absorbs the laser radiation via "inverse bremsstrahlung**"**, sustaining and growing a very hot (5,000-20,000 K) plasma ball. Used for simulating re-entry conditions and advanced propulsion.

c Resonant Laser Heating: Tuning a laser to a specific electronic or vibrational transition of a molecule (e.g., CO_2) for selective, efficient heating. This is more experimental but promising for controlling chemical reactions.

1.5.3 Microwave & Radio Frequency (RF) Heating

These methods transfer energy directly to the electrons in a gas via oscillating electromagnetic fields, often creating a plasma.

Mechanism: Free electrons in a plasma (or induced dipoles) oscillate in the alternating electric field, gaining energy and colliding with heavy particles (ions, neutrals), thereby heating the entire gas.

Advanced Techniques:

a Electron Cyclotron Resonance Heating (ECRH): A cornerstone of magnetic confinement fusion (tokamaks like ITER). Microwaves at a precise frequency (e.g., 170 GHz for ITER) are launched into a magnetically confined plasma. The frequency matches the natural gyration frequency of electrons around the magnetic field lines, leading to resonant absorption of enormous power, heating electrons to over 100 million C.

b Ion Cyclotron Resonance Heating (ICRH): Uses high-power RF waves to resonate with and directly heat ions in a fusion plasma.

c Gyrotrons & Klystrons: These are not heaters themselves but the specialized high-power sources (megawatt-level) of millimeter-wave microwaves that make ECRH possible. Their development is a major technological feat.

d Atmospheric Pressure Microwave Plasmas: Using novel cavity designs and gas flow stabilization to create stable, very hot plasmas (~10,000 K) at 1 atm for material processing and waste destruction.

1.5.4 Radiation (Broadband & Synchrotron) Heating

This involves the transfer of heat via photons, often from an extremely hot secondary source or specialized light.

Mechanism: Absorption of intense blackbody or synchrotron radiation.

Advanced Techniques:

a X-Ray and VUV Radiation from Pinch Plasmas/Z-Pinches: Massive electrical discharges (e.g., at Sandia's Z Machine) create a collapsing plasma column (a "pinch") that emits an immense pulse of soft X-rays. This radiation can be used to radioactively heat **a** secondary target (like a fusion capsule) to several million degrees in nanoseconds. This is a form of indirect drive ICF**.**

b Synchrotron Radiation Heating: Using the intense, tunable, focused X-ray beams from particle accelerator-based synchrotron light sources to deliver extreme heat loads to microscopic gas volumes or samples for fundamental high-energy-density physics research.

1.5.5 Plasma Torches / Arcjets

While conceptually older, modern implementations are highly advanced.

Mechanism: An electric arc is struck between electrodes, ionizing and heating the gas that is forced through it.

Advanced Techniques:

a Radio Frequency (RF) or Inductively Coupled Plasma (ICP) Torches (Table 1): No electrodes contact the plasma; it is heated by currents induced by a high-power RF coil surrounding the gas flow. This allows for contamination-free heating of any gas (including air, argon, oxygen) to ~10,000 K, used in aerospace testing (wind tunnels), advanced material synthesis (spherical powders), and waste vitrification.

b DC Arcjets for Space Propulsion: Use high-current arcs to heat propellants like hydrogen or ammonia for high-thrust, moderate-specific-impulse spacecraft propulsion.

1.5.6 Magnetic Compression & Ohmic Heating (Table 1)

Directly using magnetic fields to confine, compress, and heat a plasma.

Mechanism: The plasma acts as the secondary winding of a transformer (**ohmic heating**), and magnetic pressure is used to compress it adiabatically.

Advanced Technique:

a Magnetized Target Fusion (MTF) / Field-Reversed Configuration (FRC): As pursued by companies like Helion Energy and TAE Technologies. A pre-formed plasma (heated by RF or other means) is rapidly compressed by powerful magnetic pistons (liners). The adiabatic compression heats the plasma to fusion-relevant temperatures (100+ million °C) extremely quickly. This is a hybrid of magnetic and inertial confinement.

Table 1: Comparative Table of Applications and Temperature Ranges of advanced heating techniques obtained wirh the help of AI

Heating Technique	Typical Temperature Range	Key Advantage	Primary Application
Laser-Driven ICF	50 - 100+ million K	Highest power density, ignition	Inertial Confinement Fusion, HED Physics
ECRH / ICRH	10 - 200 million K	Precise, efficient, steady-state heating	Magnetic Confinement Fusion (ITER)
Laser Sustained Plasma. **Useful for Prop. thrust**	5,000 - 20,000 K	Contamination-free, high enthalpy	Hypersonic wind tunnels, propulsion simulators
RF Induct. Plasma Torch. **Useful for Prop. thrust**	6,000 - 15,000 K	Contamination-free, high gas flow rate	Material processing, testing, waste disposal
Z-Pinch Radioactive	1 - 5 million K	Immense total X-ray energy/power	HED Physics, Radiation Effects Testing
Magnetic Compression	10 - 200+ million K	Rapid, efficient scaling potential	Magnetized Target Fusion (e.g., Helion)

According to Table 1, from Google IA, the high temperature heating techniques include the two following methods:

1) Consists of a RF Induction Plasma Torch uses powerful radiofrequency (RF) electromagnetic fields to ionize a gas (like argon) into an extremely hot, high-energy plasma, creating a clean, electrode-less flame for advanced material processing like powder spheroidization, coatings, and nanoparticle synthesis, working by inducing eddy currents in the gas, heating it to thousands of degrees without direct electrical contact.

The key components and working mode include:

Radio frequency (RF) Power Supply: Generates high-frequency alternating current (e.g., 2-3 MHz).

Induction Coil: A water-cooled copper coil wrapped around a quartz tube; the RF current creates an intense, oscillating magnetic field inside.

Gas Flow: A process gas (often argon) flows through the quartz tube.

Plasma Generation: The magnetic field induces strong eddy currents in the gas, rapidly heating and ionizing it into a thermal plasma, similar to how induction heating works for metals.

Torch Head: Directs gas flow and introduces materials.

The advantages are based on:

No electrodes: Prevents contamination from electrode erosion, creating purer materials.

High temperatures: Reaches up to 10,000 Kelvin.

Versatile atmosphere**:** Can operate in air, hydrogen, helium, argon, nitrogen, or other atmospheres.

2) Consists of heating a gas by laser-sustained induced plasma which means using an intense laser beam to create a superheated, ionized gas (plasma) that then absorbs further laser energy, heating the surrounding gas to extreme temperatures, creating thrust (like for space propulsion) or enabling advanced ignition (like in engines) by delivering energy locally and efficiently. This process creates a self-sustaining plasma ball that can continuously heat the flowing gas, offering powerful, controlled heating far beyond normal combustion.

How it works:

Laser-Induced Breakdown**:** A high-power laser beam is focused into a gas (like air or a propellant-air mix). At the focal point, the energy density is so high that it ionizes the gas, creating a tiny, extremely hot spark called a Laser-Induced Plasma (LIP).

Plasma Ignition/Heating**:** This initial plasma acts as a seed, absorbing subsequent laser energy much more effectively than the cold gas, creating a stable, self-sustaining plasma "bubble" or "torch".

Energy Transfer**:** The hot plasma then transfers its immense thermal energy to the bulk gas flowing through it, heating it rapidly and to very high temperatures (thousands of degrees).

Common applications include**:**

Ignition**:** For internal combustion engines, it provides a more reliable and efficient ignition source, especially for lean (propellant-poor) mixtures, potentially improving efficiency and reducing emissions.

Propulsion**:** In space, it's used to heat propellant gas (like hydrogen) to create thrust for laser-powered rockets, offering high specific impulse.

Spectroscopy**:** Analyzing the light emitted from the plasma helps identify elements in materials (Laser-Induced Breakdown Spectroscopy - LIBS).

As a key takeaway, It's a method to concentrate laser energy into a tiny plasma spot, making that spot a powerful heat source that continuously heats a surrounding gas, enabling novel ignition and propulsion systems.

Key Scientific & Engineering Challenges include:

Coupling Efficiency: Getting the electromagnetic energy *into* the gas/plasma efficiently (e.g., avoiding reflections, finding resonance).

Containment: The hotter the gas, the more violently it expands. This requires inertial confinement (ultra-fast pulses), magnetic confinement (like tokomaks), or continuous high-flow quenching.

Diagnostics: Measuring temperature, density, and composition at these extremes is itself a cutting-edge field.

Material Survival: Protecting walls, windows (laser entry), and antennas from the intense heat and particle fluxes.

In summary, the frontier of gas heating lies in hybrid approaches (e.g., laser-initiated, magnetically compressed) and the scaling of resonant electromagnetic techniques (ECRH, ICRH) for fusion energy**,** which represents the ultimate goal of high-temperature gas physics.

1.6 The Proposed Solution

In subsection 1.4, concerning the main drawbacks inherent to NTP and NEP reactors, safety and environmental concerns, as well as engineering and operational challenges, have been discussed. According to these comments, the risk of accidents at nuclear power plants is too high and costly. The preceding comment reveals a truly disruptive decision: a radical shift in the energy paradigm that affects fundamental principles of thermodynamics; obtaining work through vacuum-induced thermal contraction achieved by cooling or heat extraction—that is, useful mechanical work is performed by extracting heat instead of adding it. The rate of useful work obtained through thermal contraction can equal the useful work obtained by adding heat. In fact, it represents twice the amount of work relative to the added heat.

In order to mitigate these risks and their consequences, a disruptive paradigm shift is proposed: replacing nuclear reactors with self-sustaining thermoelectric plants capable of supplying energy without incurring any of the risks involved in using nuclear power. The proposed techniques do not require nuclear propellant or any other propellant that would necessitate combustion. They are technically accessible and cost-effective.

The reason this principle hasn't been applied earlier, that is, at the beginning of the industrial era more than two centuries ago (when the fundamental principles of thermodynamics were formulated), is due to the neglect of elementary physical concepts. This is probably because the solution adopted was based on heat transfer from a given potential to a lower one to produce work through adiabatic expansion, without considering other possible principles such as reverse heat transfer—from lower to higher temperatures—which gives rise to work by thermal contraction, one of the fundamental pillars of this proposal. This technique leads to a reconsideration of the energy balances that affect the first law of thermodynamics and exergy, or available useful energy.

1.6.1 The Self-Sustaining Power Machine

The concept of "Self-Sustaining Power Machines" (SSPMs) has been introduced and described in previous references [11-20]. In short, it consists of a disruptive, technically and economically viable alternative solution that allows for the intensive generation and/or dissipation of heat in cosmic environments, in addition to direct

radiation into deep space. This involves the implementation of heat sinks using reverse Brayton cycles (RBCs) powered by SSPMs.

1.6.2 The proposed power units based on Pulses-based Gas Turbines [15], Patent [28]

Every PU consists of a a disruptive Self-Sustaining Power Machine (SSPM) composed of cascaded power units (PUs). Each PU consists of a Pulse Gas Turbine (**PGT**). The prototyping design task involves a singular thermal cycle (sVsVs) associated to each PU, characterized by doing work by:

(a) Expansion of a Thermal Working Fluid (**TWF**) due to previous heat addition,

(b) Contraction of a TWF previously cooled by heat extraction and,

(c) Upgrading recovered heat by increasing thermal potential by heat superposition techniques, and

(d) Efficient use of the heat recovered from each upstream PU to feed the first PU downstream.

The fact of achieving useful mechanical work with the above-mentioned procedures by adding only heat to produce expansion work undergoes an excess of useful mechanical work greater than the amount of added heat, which gives rise to a SSPM enabled to defy Perpetual Motion Machines (PMM) of second kind.

In the proposed configuration, the heat released from each PU due to the cooling of the TWF is efficiently recovered and reused in the first PU in the cascade. Results have been verified through two case studies carried out on a SSPM simulated prototype [15], being conducted using air and helium as real gases.

The significant differences of the presented technology based on the proposed PGT technology [15], compared to Rankine cycles, ORCs, and Brayton cycles used in the most advanced power reactors are summarized in the following points:

There are no phase changes of the TWF (such as helium, dry nitrogen, dry air, among other TWFs, which means that the heats of vaporization and condensation are not present.

The tasks of adding and extracting heat to/from the cycle are carried out at constant volume. This is possible by alternately operating with two or more heating and cooling isochoric reservoirs, which operate under forced convection heat transfer.

No conventional feed pumps are required because there are no phase changes. Instead, a low-pressure TWF feed compressor is used, where the low-pressure compression is due to the fact that during the time the working fluid is being pumped from a low-temperature fluid reservoir to a high-temperature fluid reservoir, it exhibits suction and discharge pressures very close to each other.

Cooling turbine blades is not required in any case.

An installation based on a cascade coupling structure of a group of PGTs with respect to the heat transfer fluid (HTF) temperature mechanically coupled on the same rotating shaft contributes to an effective waste heat recovery system based on the following facts:

1 Effective recovering and use of low-grade heat exhausted from the connected upstream turbines.

2 The thermal efficiency of a PGT cycle is independent of the range between high and low temperatures since it does not obey Carnot constraints. Contrary to Carnot, indeed, efficiency is higher for low-temperature ranges (T_H-T_L) which implies high temperature ratios (T_L/T_H). This characteristic also contributes to the increase of the residual heat utilization factor.

Given that the efficiency of each individual PGT is significantly higher than in conventional Rankine cycles-based steam turbines, associated to the fact that the heat utilization factor is also greater, the overall efficiency is significantly increased.

In summary, the key innovations and contraction, the efficient recovery and reuse of contraction heat, and the strategic selection of the TWF and number of PUs, consist of the utilization of thermal contraction to generate work, the specialized thermal cycles that leverage expansion working fluids - all of which contribute to the SSPM's remarkable improvements in thermal efficiency and self-sufficiency. Consequently, the proposed power and propulsion architecture presents characteristics that challenge the most advanced and modern nuclear reactors.

1.7 Purpose & Roadmap

With the aim of providing technical means for energy supply to assist all types of domestic and industrial activities in all areas associated with the industrial fabric required for specific in-situ tasks related to the exploitation of extraterrestrial resources, the following sections will describe two key topics: energy

self-sufficiency and space propulsion for interplanetary transport. Therefore, the work is organized according to the following structure:

Section 2, Modeling a SSPM with cascaded Pulse-based Gas Turbines based on references [11-23] and [24-29],

Section 3, Modeling of the Spacecraft Propulsion System.

Section 4, Analysis of results

Section 5, Overall Conclusions and Implications

2. Modelling a SSPM with cascaded Pulse-based Gas Turbines [15], [29]

The proposed electric power generation plant consists of a cascade of power units made up of gas turbines operating on barothermal impulses driven by known thermal cycles of the sVsVs type.

2.1 Brief Description of the PGT Structure and its Operating Modes

The Power Generation Units (PUs) for the proposed Self-Powered Power Plant (SPPP) prototype are based on the PGT (Pulsed Gas Turbine) technology patented under application number P202000032 and publication number ES2851381. The PGT scheme is illustrated in Figure 1a.

The PGT structure is composed at least of four main subsystems:

- Heat supply system, responsible for heating the thermal working fluid (TWF) which gives rise to puss forces enabled to do useful expansion work,

- Heat extraction system, responsible for cooling the TWF which gives rise to a vacuum responsible for pull forces enabled to do useful contraction work,

- Heat recovery system enabled to recover the cooling heat released from the heat extraction system which will be feed back to the internal heat supply system,

- Pulse-based gas turbines (PGT) itself,

- Thermal working fluid pump feeding system,

- Systems circuits and controlled valves and, - advanced control equipment.

Figure 1(a) depicts an expansion-contraction heat scheduling scheme equipped with two reservoirs for heating and cooling, which operate in an alternating and intermittent sequence. Figure 1(b) presents a symbolic scheme representing each power unit within the self-powered power plant.

The PGT prototype shown in Figure 1(a) consists of one or more closed-circuit gas turbines designed for installation in power plants, where they are coupled via a common shaft to all rotating machines in the system. Each PGT operates intermittently based on barothermal pulses. These pulses are generated within dedicated reservoirs and are of two types:

Positive barothermal pulses involve a pressure increase above an equilibrium (reference) pressure, associated with the temperature rise from isochoric heating.

Negative barothermal pulses involve a pressure decrease below the equilibrium pressure, associated with the temperature drop from isochoric cooling.

These pulses are applied to the gas turbine from high-pressure and low-pressure reservoirs, respectively, driving its operation.

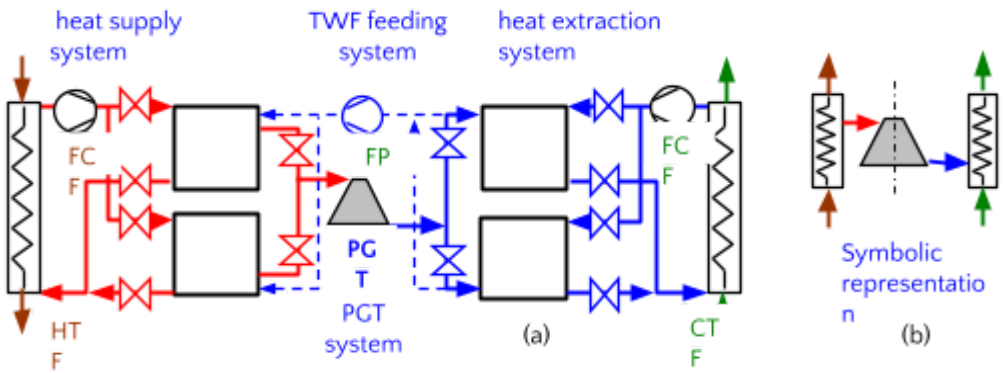

Figure 1: Illustration of the PGT based on the patent application number P202000032 and publication number ES2851381, [15], [29]. Figure 1(a) depicts the main subsystems including the heat supply system, the heat extraction system, the TWF feeding system and the PGT machine. Figure 1 (b) depicts illustrates the symbol used to represent the main subsystems depicted in Figure 1(a).

To facilitate a clear and concise description of the operating modes of a PGT-based PU with a sVsVs-type thermal cycle, refer to Fig.

Figures 2(a) and 2(b) depict the following processes for the first pair of reservoirs:

Open-Isochoric heat addition in reservoir A.

Open-Isochoric heat extraction in reservoir B.

Figures 2(c) and 2(d) show the corresponding processes for the second pair:

Open-Isochoric heat addition in reservoir C.

Open-Isochoric heat extraction in reservoir D.

The pressure-volume (p-V) diagrams for the sVsVs cycles executed sequentially in reservoir pairs A-B and C-D are presented in Figures 2(e) and 2(f). Each complete operating cycle of the PU consists of these two sVsVs cycles.

Figures 2(g) and 2(h) show pressure-time diagrams for both reservoir pairs. They illustrate the net pressure, defined as the difference between the pressures in reservoirs A and B for the first sVsVs cycle, and between reservoirs C and D for the second.

The concatenation of these sVsVs cycles is illustrated in Figure 3, which plots the resulting pressure pulses over time for one full PGT cycle (comprising two sVsVs thermal cycles).

The configuration requires at least two reservoirs to accumulate thermally active fluid (TWF) for two key reasons:

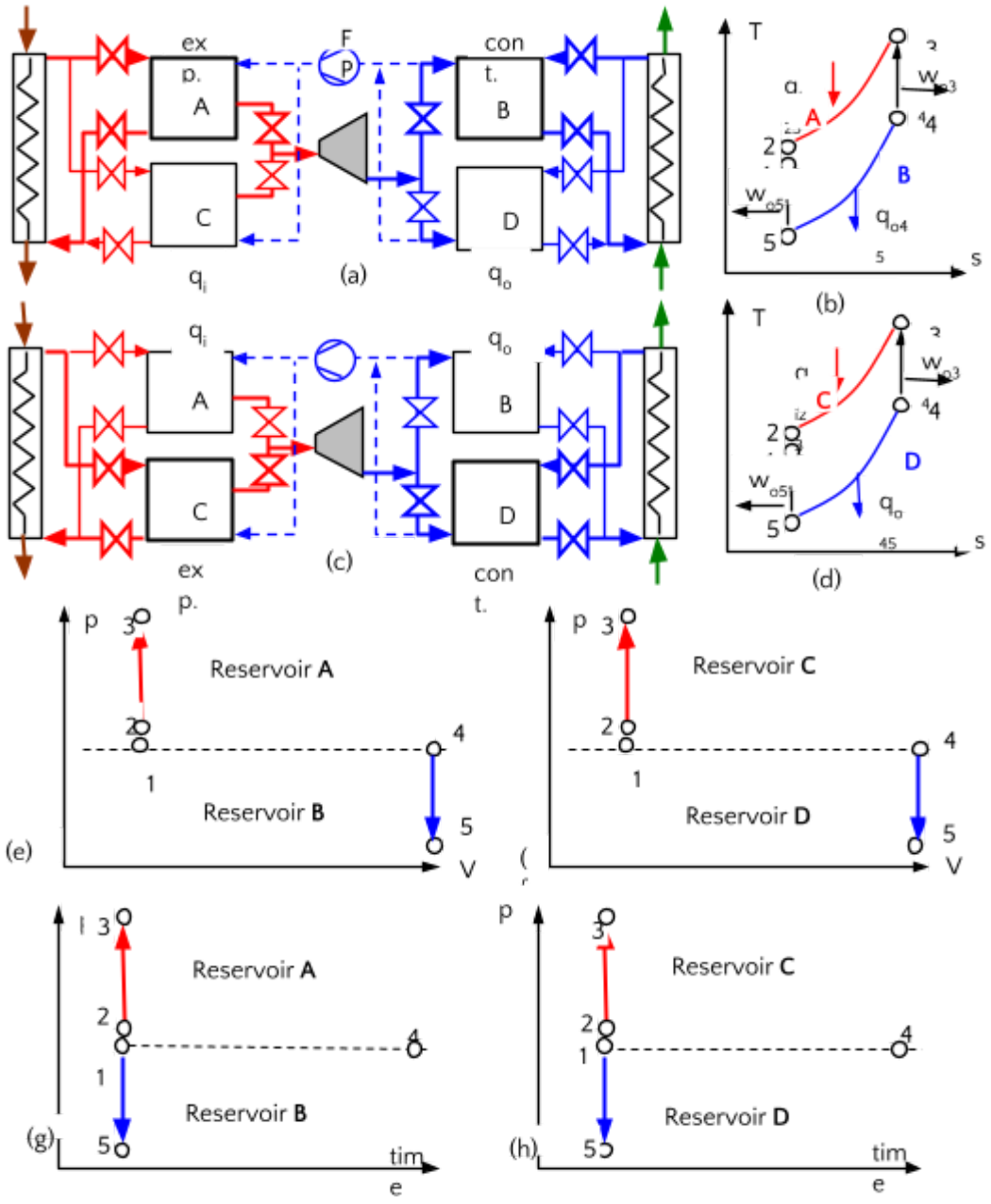

Figure 2: PU scheme to illustrate the operating modes

High-Pressure/Temperature Pulses (Positive pressure pulses):

Reservoirs at the heat source accumulate heated TWF at constant volume, enabling the intermittent generation of high-pressure, high-temperature (barothermal) pulses at the gas turbine inlet.

Low-Pressure/Temperature Pulses (negative pressure pulses):

Reservoirs at the heat sink accumulate cooled TWF at constant volume, enabling the intermittent generation of low-pressure, low-temperature pulses. These create synchronized negative pressure pulses in the gas turbine's evacuation zone.

In one viable design, each high-pressure barothermal pulse applied at the turbine inlet is synchronized with a corresponding negative pressure pulse applied in the evacuation zone.

A complementary process occurs on the low-pressure side. After a reservoir is cooled and contracts, it is connected to the turbine's evacuation zone. This connection increases its pressure from the minimum cooling pressure back to the intermediate reference level. It is then isolated, allowing the next cooled reservoir to take its

place. Consequently, when one reservoir is in this intake/compression state, its counterpart is in the isochoric cooling phase. This operating behavior is depicted in Fig. 3, where expansion and contraction pressure are depicted simultaneously giving rise to a greater difference of pressure between positive and negative pressure.

Finally, Figures 2(b) and 2(d) illustrate the sVsVs cycle on temperature-entropy (T-s) diagrams, highlighting the active heating and cooling phases. These processes are also summarized in Table 2. The cycle consists of two sequential heat transfer processes: isochoric heat addition (which increases temperature and pressure, producing expansion work) and isochoric heat extraction (which decreases temperature and pressure, producing contraction work). A detailed cycle analysis will be provided in the next section.

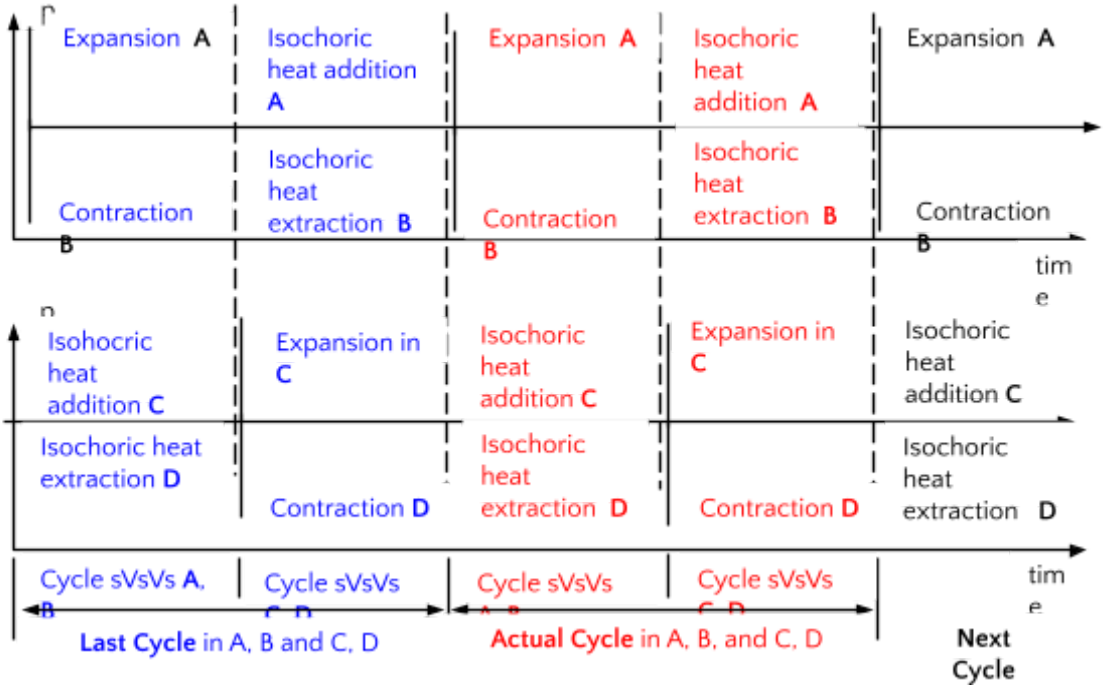

Figure 3: Pressure-time diagrams of the thermal cycle sVsVs and cycle timing synchronization

Simultaneously applying positive and negative pressure pulses to the high and low-pressure zones of the barothermal-pulse gas turbine creates a significant pressure differential between its inlet and outlet. This generates a very high initial torque at the start of each barothermal pulse, which attenuates as the Thermodynamic Working Fluid (TWF) expands within the turbine.

In an alternative design, a negative pressure pulse is not applied to the evacuation zone during the heat extraction phase. Instead, heat is rejected to the sink at the reference pressure and temperature. When only positive pressure pulses are applied at the inlet, the achieved pressure differential is only that between the inlet and the equilibrium pressure of the heat sink. Consequently, the torque produced per pulse is lower than in the dual-pulse (positive/negative) configuration.

Table 2 sVsVs thermal cycle execution sequence

sp	Process task	Sequential sVsVs cycle processes	Thermal-model
1-2	Feed pump work in	Open adiabatic-isentropic	$w_{i12} = \Delta h_{12}$
2-3	Heating the TWF	Open isochoric heat addition	$q_{i23} = \Delta h_{23}$
3-4	Expansion work out	Open adiabatic-isentropic expansion	$w_{o\exp 34} = \Delta h_{34}$
4-5	Cooling the TWF	Open isochoric heat extraction	$q_{o45} = \Delta h_{45}$
5-1	Contraction work out	Open adiabatic-isentropic contraction	$w_{ocont51} = \Delta h_{51}$

Within each high-pressure reservoir, the TWF is held at high temperature and pressure. When released in a pulse, it expands adiabatically through the turbine. Notably, this adiabatic expansion approximates a quasi-isothermal process because:

The heat accumulated in the metal of each isochoric heating reservoir and its associated heat exchanger transfers heat *to* the TWF during expansion.

Conversely, each isochoric cooling reservoir and its cooler transfers heat *from* the heat-extraction fluid during expansion.

This process generates useful mechanical work, which can then be converted into electrical energy.

In Table 2 it is depicted the sVsVs cycle on temperature-entropy (T-s) diagrams, highlighting the active heating and cooling phases by means of a sVsVs thermal cycle execution sequence.

2.2 Operating Principle

The system operates using alternating thermal reservoirs. Generally, when a high-pressure thermal fluid reservoir—pressurized by constant-volume (isochoric) heating—is connected to the gas turbine, the working fluid expands.

This expansion drives the turbine and decreases the fluid's pressure to an intermediate reference level. At this point, the reservoir is isolated from the turbine. A second, pre-heated reservoir then comes into operation, ensuring a continuous power output. Thus, while one reservoir is in the expansion phase, others are simultaneously undergoing pen isochoric heating.

2.2.1 Key Advantages Over Conventional Cycles:

The proposed Pulsed Gas Turbine (PGT) technology offers several distinct advantages:

1 No Phase Change**:** The Thermodynamic Working Fluid (TWF)—such as helium, dry nitrogen, or dry air—remains in a single gaseous phase. This eliminates the latent heats of vaporization and condensation, simplifying system design.

2 Open -Isochoric Heat Transfer: Heat addition and rejection occur at constant volume within dedicated, alternately operated reservoirs. This is achieved via forced convection heat transfer.

3 Reduced Cooling Demands: Turbine blade cooling is not required for operating temperatures below approximately 1200 K.

4 Cascaded Waste Heat Recovery: Multiple PGT units can be mechanically coupled on a single shaft in a cascade structure, sequenced according to the Heat Transfer Fluid (HTF) temperature gradient. This creates an effective waste heat recovery system because:

a It efficiently recovers and utilizes low-grade heat exhaust from upstream turbine stages.

b The thermal efficiency of a PGT cycle is not governed by Carnot constraints. Unlike Carnot cycles, PGT efficiency is higher for smaller temperature ranges, which correspond to high temperature ratios. This characteristic significantly enhances the residual heat utilization factor.

Given that the individual efficiency of each PGT unit is substantially higher than that of conventional Rankine-based turbines, and coupled with a superior heat utilization factor, the overall system efficiency is markedly increased. However, even so, self-sufficient capabilities require adding another strategy that deals largely with cascade heat recovery.

2.3 PGT-based sVsVs Cycle

Let us begin by clarifying the acronym for the thermal cycle under study: the sVsVs cycle, implemented in a Pulse-based Gas Turbine (PGT) system. The letters in the acronym denote the thermodynamic transformations between successive state points. Here, "s" represents an open isentropic (constant entropy) process, and "V" represents an open-isochoric (constant specific volume) process. Thus, sVsVs describes a sequence of five processes: isentropic, open-isochoric, isentropic, open-isochoric, and isentropic.

Processes of the sVsVs Cycle:

The cycle, illustrated in Table 2, consists of the following transformations between state points:

Process 1–2: Open isentropic compression. TWF is transferred from the cold TWF reservoir to the hot TWF reservoir.

Process 2–3: Closed isochoric heat addition. Heat addition is carried out by means of TWF closed process recirculation under forced heat transfer

Process 3–4: Open isentropic expansion. Mechanical work is performed by hot TWF open process expansion.

Process 4–5: Closed isochoric heat extraction (no heat rejection). Heat extraction (cooling) is carried out by means of TWF closed process recirculation under forced heat transfer.

Process 5–1: Open isentropic contraction. Mechanical work is performed by cold TWF open process contraction.

These processes are described in detail below:

Process 1–2:

This corresponds to an open, adiabatic, and isentropic compression process driven by a feed pump or gas compressor. It is classified as an "open" process because it involves mass transfer. The work input to the compressor for this adiabatic-isentropic process is given by:

$$w_{i12} = w_{iFP} = \Delta h_{12} = h_2 - h_1 = Cp \cdot (T_2 - T_1) \quad (1)$$

Process 2–3:

Correspond to a open-isochoric heat addition process in which the working fluid is heated.

$$q_{i23} = \Delta h_{23} = h_3 - h_2 = Cp \cdot (T_3 - T_2) \quad (2)$$

Process 3–4:

Correspond to an open adiabatic expansion process in the PGT which undergoes mass transfer while volume increases. Thus the thermal energy in the form of enthalpy is converted into mechanical work, provided that the PGT rotates freely doing expansion work.

$$w_{o34} = w_{o\exp 34} = h_3 - h_4 = \Delta h_{34} = Cp \cdot (T_3 - T_4) \quad (3)$$

Process 4–5:

Correspond to a open-isochoric heat addition process in which the working fluid is heated without work done because of the constant volume process

$$q_{o45} = \Delta h_{45} = h_4 - h_5 = Cp \cdot (T_4 - T_5) \quad (4)$$

Process 5–1:

Correspond to open adiabatic contraction-based compression process. Thus the thermal energy in the form of enthalpy is converted into mechanical work by contraction (TWF volume decreases in the cold PGT reservoir), provided that the PGT can move freely to permit the contraction-based compression work.

$$|w_{o51}| = |w_{ocont51}| = |h_5 - h_1| = Cp \cdot |(T_5 - T_1)| = Cp(T_1 - T_5) \quad (5)$$

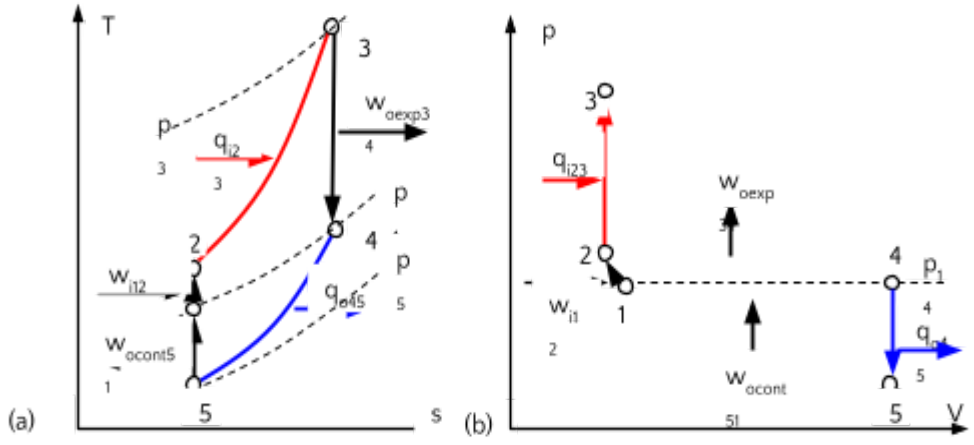

Figure 4: Single PGT-sVsVs hybrid (closed & open processes) thermal cycle. (a): T-s diagram. (b): p-V diagram

The sVsVs thermal cycle is hybrid due to be composed by closed and open processes. While heat transfer is carried out by adding and extracting heat by means of isochoric closed processes, the rest of processes involving

work undergo mass transfer. Consequently, the open process-based heat-work interactions are modeled by using enthalpies.

2.4 sVsVs analysis

The analysis of the 4CP VsVs is based on the first law, so that the energy transfer flows include the following energy balances derived from the previous section:

Input heat:

heat added at closed isochoric heat transfer process

$$q_{i23} = \Delta h_{32} = Cp \cdot (T_3 - T_2) \tag{6}$$

Output heat

heat extracted at closed isochoric heat transfer process

$$q_{o45} = \Delta h_{45} = Cp \cdot (T_4 - T_5) \tag{7}$$

Input work

The input work in the sVsVs cycle is due to the pumping effort of the feed compressor. In order to simplify the analysis without loss of generality, the amount of work done on the feed compressor to transfer the working fluid from the cold reservoirs to the hot reservoirs is

$$w_{i12} = \Delta h_{21} = h_2 - h_1 = Cp \cdot (T_2 - T_1) \tag{8}$$

Output work

The work done by expansion along the process 2-3 due to the isochoric heat added is

$$w_{o34} = w_{o\exp 34} = \Delta h_{34} = Cp \cdot (T_3 - T_4) \tag{9}$$

The work done by contraction along the process 5-1 due to the isochoric heat extracted is

$$w_{o51} = w_{ocont51} = \Delta h_{51} = Cp \cdot (T_1 - T_5) \tag{10}$$

Net useful work

$$w_n = w_{o\exp 34} + |\, w_{ocont51}\,| - \Delta h_{12} = \Delta h_{34} + \Delta h_{51} - \Delta h_{12} \tag{11}$$

Therefore, the thermal efficiency is given by the ratio of the mechanical work to the input heat, yielding

$$\eta_{th} = \frac{w_n}{q_i} = \frac{w_{o34} + |\, w_{o51}\,| - \Delta h_{12}}{\Delta u_{32}} = \frac{\Delta h_{34} + \Delta h_{51} - \Delta h_{12}}{Cv \cdot (T_2 - T_1)} = \tag{12}$$

2.5 Design considerations to achieve a high amount of contraction work with respect to expansion work

In order to achieve a similar structure in dimensional terms between the PGT-based rotary actuators endowed with the ability to convert heat to work with the same actuator volume at the cost of different temperatures and pressures, a constant temperature jump or drop pa temperature (T_{drop}) is used between each of the PUs that make up the PU cascade.

Each Power Unit (PU) completes one PGT cycle by executing two sequential sVsVs thermal cycles. These cycles operate in a complementary manner: while one sVsVs cycle performs mechanical work through expansion and contraction, the other simultaneously undergoes heat addition and extraction.

To proceed with the study of the SSPM, it is essential to characterize each PU based on the properties of its thermal cycle. This analysis focuses on the behaviour of the PGT-sVsVs cycle with respect to the isochoric temperature drop, defined as $T_D = T_3 - T_1$. The goal is to identify a constant temperature drop that ensure acceptable performance for the complete SSPM which involves each PU within an operating range suitable for cascade integration downstream in the SSPM.

The ratio RW of the contraction to the expansion works for every PU depends on the T_D so that

$$WR = \frac{w_{ocont}}{w_{o\exp}} \tag{13}$$

The ratio of contraction to expansion work cannot be equal to one. If the temperature drop between each cascaded PU approaches zero, the ratio WR tends to one. In this limit, T_1=T_3, meaning no heat transfer occurs, and consequently no power can be developed. As T_3 approaches T_1, the amount of useful work obtained from cooling increases, which enhances thermal efficiency. However, achieving this requires increasing the number of PUs. Consequently, it is necessary to determine an optimal temperature jump that maximizes net profit by balancing improved efficiency against the higher cost associated with adding more PUs.

2.6 Integration of the PGT sVsVs cycle into a cascade of PUs enabled to implement a SSPM [15]

A systematic methodology to implement a cascaded group of PUs operating with a constant temperature difference TD is proposed: The cases studies comprehend four T_D values applied on the study of 4 SSPMs-based case studies operating by means of thermal cycles of the type PGT-sVsVs, where top temperature T_3 is fixed in 1000 K for the first PU of each cascaded SSPM cascade and the corresponding temperature T_1 according the chosen TD. By processing the data of Table 2 according to the thermodynamic model of the proposed thermal cycle described along equations (1-6 and 7-12), a useful set of data is obtained as results of the analysis, as function of the constant T_D for each case which is depicted in Table 3. The mentioned results include the high and low temperatures, the specific flows of input heat and output heat, as well as useful mechanical work, and with the aim of comparison purposes the thermal efficiency and Carnot factor is also depicted.

The cascaded PUs-based structure is configured according to the Fig. 2(a) and 2(c). Observing Fig. 5 it can be noted that while the heat supply system includes a set of cascaded heat exchangers to supply heat to all cascaded PUs of the SSPM, the cooling heat from the reservoirs responsible for the vacuum is extracted from them in a cascade and recovered to be fed back into the internal heat supply system. The unique circuit responsible for the circulation of the HTF enabled to add and extract heat to/from the hot and cold reservoirs is essential to achieving self-sustainability capabilities.

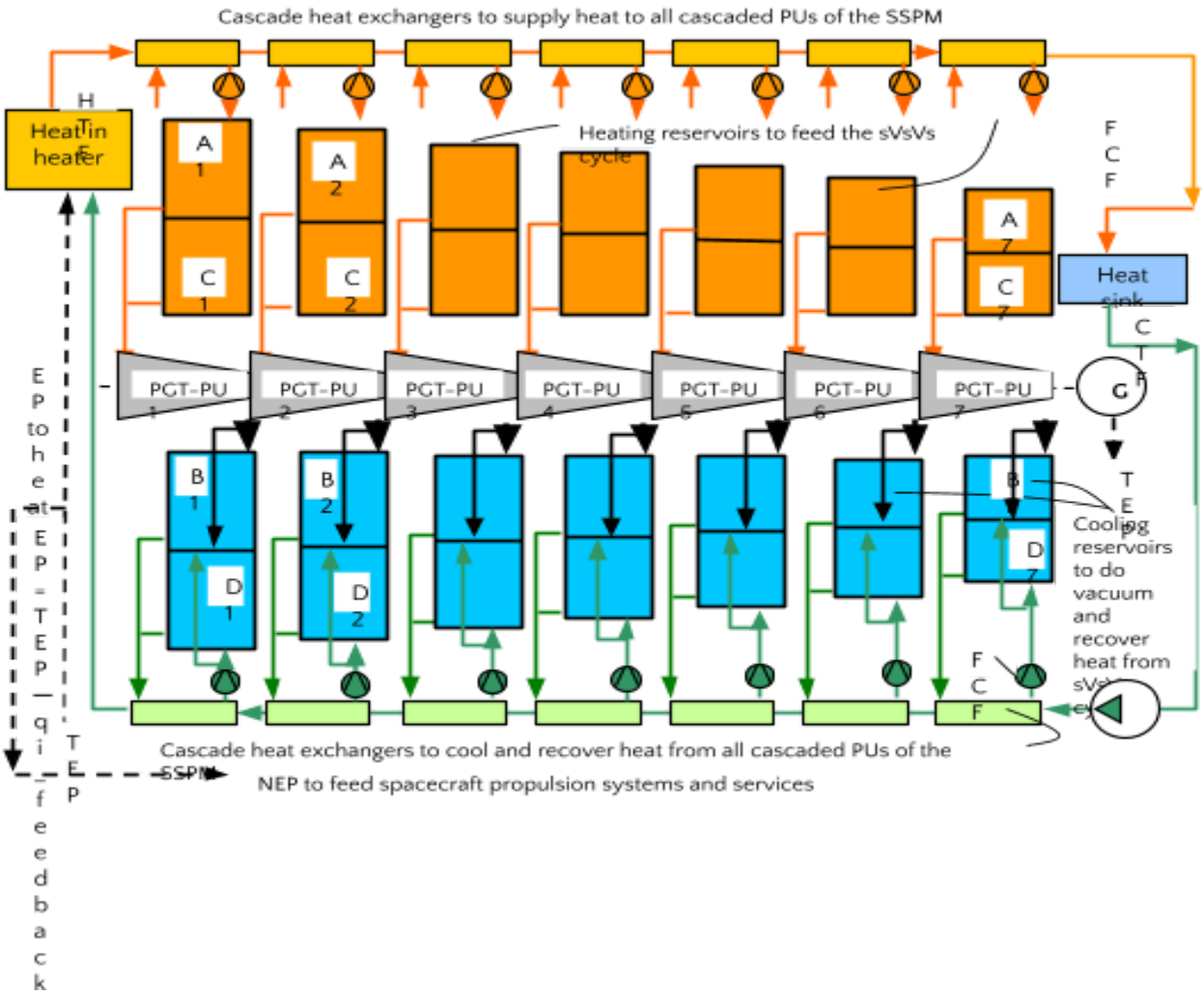

Figure 5: Structure of a SSPM composed of seven cascaded PGT-based PUs, showing some of the most significant components: [15], [28], [29].

Fig. 5 illustrates the main components of a SSPM composed of cascaded PUs made of rotary actuators based on PGTs [15], [28] and [29]. Among the main parts, each PU shows:

- Two TWF's reservoirs for heat addition

- Heat addition piping responsible for raising the TWF pressure and temperature by means of the HTF circulation

- TWF recirculation ducts via a recirculation compressor for heat addition to the TWF by forced convection

- A gas turbine-based rotary actuator that operates using pressure and temperature pulses (PGT)

- Two TWF reservoirs for heat extraction cooling

- HTF extraction circuit piping or ducts from the reservoirs responsible for generating a vacuum

- TWF recirculation circuit piping or ducts via a recalculating compressor for heat extraction from the TWF by forced convection

- Recirculation pump for HTF (thermal oil or equivalent)

- Recirculation rotary feed compressors to activate forced convection heat transfer to/from the HTF (thermal oil) to/from the TWF of any PU of the SSPM.

- Feed Pump for each PU —not represented in the figure

With regard to the structure depicted in Fig. 5 it is worth noting that the volume of the TWF tanks, both hot and cold, for each power unit (PU) is different; however, the volume of each PGT-based rotary actuator for each PU is identical. This design strategy allows for a significant reduction in the manufacturing and maintenance costs of

the rotating machines, as they are identical because they only have to withstand relatively small temperature and pressure changes, which implies minimal thermal variations under steady-state operating conditions.

Therefore, the next section on design addresses the proposed case studies that take into account the aforementioned observation.

Since the rocket propulsion system power technology based on SSPM must replace nuclear power, which will be the power source for rocket propulsion systems for space exploration of the solar system, we will call such self-sustaining power systems "self-sustaining power generators" (SSPG).

2.7 Case studies on SSPMs

In the next tables from 3 to 10, computation data and results for helium as working fluid is depicted. Four case studies are analyzed and compared. Real TWF data used belongs to the database provided by Lemmon E. W., et all, (2007), [22]. In Table 3, 5, 7 and 9, sVsVs cycles processing data is depicted, while in Tables 4, 6, 8 and 10 main results from cycle's data are depicted. For all studied cases the top temperature 100 (K) is chosen. Nevertheless, different temperature differences are considered (50-75-100 and 150 K respectively). Therefore the case illustrated by tables 3 and 4 (data cycle processing and results) operate with a T_D of 50 (K), which includes 13 PUs. Tables 5 and 6 operate with a T_D of 75 (K), includes 9 PUs. Tables 7 and 8 operate with a T_D of 100 (K) which includes 7 PUs and tables 9 and 10 operate with a T_D of 150 (K) which includes 4 PUs. Considering helium as TWF, thermal and mechanical losses are grouped as losses factor (LF) = 0.9 which is interpreted as a thermal efficiency of 90 (%), while isentropic losses (I_eff) are assumed as 0.9 which contributes to an efficiency of 90 (%). Consequently, total losses will account for the product 0.9 *0.9 =0,81 (%).

2.7.1 SSPM composed by 13 PUs operating with a PGT-sVsVs thermal cycle with helium and T_D: 50 K

The number of PUs in each SSPM is associated with the operating temperature range (T_H-T_L =1000-350K) and the temperature jump **T_D** between each cascaded PU, such that if an operating temperature range between 1000 and 350 (K) is chosen, the number of possible 50 K jumps is the ratio between range and temperature jump; that is (1000-350)/50 = 13 PUs. Therefore Table 3 depicts the results for each PU.

Table 3 Processed data for a SSPM composed by 13 cascaded PUs into the temperature range of 100-350 K.

sp	T(K)	p(bar)	v(m^3/kg)	u(kJ/kg)	h(kJ/kg)	s(kJ/kg. K)
			PU 1; T_D = 50 K			
1	950.00	20.00	0.9891	2966.20	4944.50	27.772
2	959.10	20.50	0.9747	2995.80	4999.39	27.772
3	1000.00	21.36	0.9747	3122.10	5204.50	27.901
4	973.96	20.00	1.0140	3040.90	5082.46	27.901
5	950.00	20.00	0.9891	2966.20	4944.50	27.772
			PU 2; TD = 50 K			
1	900.00	20.00	0.9372	2810.40	4684.90	27.491
2	908.94	20.50	0.9235	2838.30	4736.57	27.491
3	950.00	21.43	0.9235	2966.30	4944.90	27.629
4	924.25	20.00	0.9624	2886.00	4824.21	27.629
5	884.00	19.13	0.9624	2760.50	4601.50	27.491
			PU 3; TD = 50 K			
1	640.00	2.00	4.4146	1999.40	3329.60	950.00
2	850.00	20.00	0.8853	2654.60	4425.30	27.194
3	858.40	20.50	0.8723	2680.90	4473.86	27.194
4	900.00	21.49	0.8723	2810.50	4685.30	27.342
5	874.55	20.00	0.9108	2731.10	4565.96	27.342
			PU 4; TD = 50 K			
1	800.00	20.00	0.8334	2498.80	4165.70	26.879

2	807.87	20.50	0.8211	2523.40	4211.26	26.879
3	850.00	21.57	0.8211	2654.70	4425.70	27.037
4	824.65	20.00	0.8590	2575.70	4306.90	27.037
5	784.00	19.02	0.8590	2448.90	4082.30	26.879
			PU 5; TD = 50 K			
1	750.00	20.00	0.7815	2343.00	3906.10	26.544
2	757.39	20.50	0.7700	2366.10	3948.88	26.544
3	800.00	21.65	0.7700	2498.90	4166.20	26.715
4	775.06	20.00	0.8075	2421.10	4049.20	26.715
5	734.00	18.94	0.8075	2293.10	3822.70	26.544
			PU 6; TD = 50 K			
1	700.00	20.00	0.7296	2187.20	3646.50	26.186
2	706.93	20.50	0.7189	2208.80	3686.61	26.186
3	750.00	21.75	0.7189	2343.10	3906.60	26.370
4	725.23	20.00	0.7558	2265.90	3790.41	26.370
5	683.70	18.86	0.7558	2136.40	3561.50	26.186
			PU 7; TD = 50 K			
1	650.00	20.00	0.677730	2031.40	3386.90	25.801
2	656.40	20.50	0.667750	2051.40	3424.01	25.801
3	700.00	21.86	0.667750	2187.30	3647.00	26.002
4	675.61	20.00	0.7043	2111.20	3532.52	26.002
5	633.40	18.75	0.7043	1979.60	3300.30	25.801
			PU 8; TD = 50 K			
1	600.00	20.00	0.6258	1875.60	3127.30	25.386
2	605.98	20.50	0.6167	1894.20	3161.97	25.386
3	650.00	21.99	0.6167	2031.50	3387.50	25.605
4	625.88	20.00	0.6527	1956.20	3274.19	25.605
5	583.40	18.64	0.6527	1823.80	3040.70	25.386
			PU 9; TD = 50 K			
1	550.00	20.00	0.5740	1719.80	2867.70	24.934
2	555.45	20.50	0.5655	1736.80	2899.26	24.934
3	600.00	22.14	0.5655	1875.70	3127.90	25.174
4	576.02	20.00	0.6010	1800.90	3015.31	25.174
5	533.40	18.52	0.6010	1668.00	2781.00	24.934
			PU 10; TD = 50 K			
1	500.00	20.00	0.5221	1563.90	2608.10	24.439
2	504.94	20.50	0.5144	1579.40	2636.77	24.439
3	550.00	22.33	0.5144	1719.90	2868.40	24.706
4	526.37	20.00	0.5494	1646.10	2757.34	24.706

5	483.20	18.36	0.5494	1511.50	2520.30	24.439
			PU 11; TD = 50 K			
1	450.00	20.00	0.4702	1408.10	2348.50	23.892
2	454.45	20.50	0.4633	1422.00	2374.28	23.892
3	500.00	22.55	0.4633	1564.10	2608.90	24.190
4	476.57	20.00	0.4978	1490.90	2498.65	24.190
5	433.00	18.17	0.4978	1355.00	2259.60	23.892
			PU 12; T_D = 50 K			
1	400.00	20.00	0.4183	1252.20	2088.80	23.281
2	404.00	20.50	0.4122	1264.70	2112.13	23.281
3	450.00	22.83	0.4122	1408.20	2349.40	23.617
4	426.78	20.00	0.4461	1335.70	2240.05	23.617
5	383.20	17.96	0.4461	1199.80	2000.90	23.281
			PU 13; TD = 50 K			
1	350.00	20.00	0.3664	1096.40	1829.20	22.587
2	353.46	20.50	0.3611	1107.20	1849.31	22.587
3	400.00	23.19	0.3611	1252.40	2089.90	22.973
4	377.00	20.00	0.3944	1180.50	1981.45	22.973
5	333.10	17.68	0.3944	1043.60	1740.70	22.587

Table 4 (a): Partial results of the cascaded PUs (1-7) from data processed in Table 3

PU	1	2	3	4	5	6	7
LF(%)	0.90	0.90	0.90	0.90	0.90	0.90	0.90
Is_eff(%)	0.90	0.90	0.90	0.90	0.90	0.90	0.90
T_3_sVsVs	1000.00	950.00	900.00	850.00	800.00	750.00	700.00
T_1_sVsVs	950.00	900.00	850.00	800.00	750.00	706.93	650.00
qi_top/PU(kJ/kg)	205.11	208.33	211.44	214.44	217.32	219.99	222.99
qo_34(kJ/kg)	218.66	222.71	224.06	224.60	226.50	228.91	232.22
q_rec(kJ/kg)	218.66	222.71	224.06	224.60	226.50	228.91	232.22
mean_rec_T(K)	961.98	912.13	862.28	812.33	762.53	712.62	662.81
wi12(kJ/kg)	54.89	51.67	48.56	45.56	42.78	40.11	37.11
wo23(kJ/kg)	109.84	108.62	107.41	106.92	105.30	104.57	103.03
wo41(kJ/kg)	72.63	75.06	75.06	75.06	75.06	76.50	77.94
RW(%)	66.13	69.10	69.88	70.20	71.28	73.16	75.65
wn(kJ/kg)-PE/cy	127.58	132.01	133.91	136.42	137.58	140.96	143.86
η_th/PU	62.20	63.37	63.33	63.62	63.31	64.08	64.51
Vreserv(m3/kg)/PU)	0.9747	0.9235	0.8723	0.8211	0.7700	0.7189	0.6678
Vtot (m3/kg)/PU)	1.0140	0.9624	0.9108	0.8590	0.8075	0.7558	0.7043
ΔV_turb(m^3)	0.0393	0.0389	0.0385	0.0379	0.0375	0.0369	0.0366
pref(bar)/PU	20.00	20.00	20.00	20.00	20.00	20.00	20.00
Δp (bar)/(PU-cycle)	0.86	0.93	0.99	1.07	1.15	1.25	1.36
qi_feedback (PU1)=h_3-h_5(kJ/kg-cycle							

Useful output work=$\sum w_n$ (kJ/kg-cycle)

Table 4(b): Partial results of the cascaded PUs (8-13) from data processed in Table 3

PU	8	9	10	11	12	13	Total
LF(%)	0.90	0.90	0.90	0.90	0.90	0.90	0.90
Is_eff(%)	0.90	0.90	0.90	0.90	0.90	0.90	0.90
T_3_sVsVs	650.00	600.00	550.00	500.00	450.00	400.00	
T_1_sVsVs	600.00	550.00	500.00	450.00	400.00	350.00	
qi_(h_3-h_2)/PU(kJ/kg)	225.53	228.64	231.63	234.62	237.27	240.59	2897.92
q_{o_34}(kJ/kg)	233.49	234.31	237.04	239.05	239.15	240.75	3001.45
$q_{\_rec}$(kJ/kg)	233.49	234.31	237.04	239.05	239.15	240.75	2431.17
mean_rec_T(K)	612.94	563.01	513.19	463.29	413.39	363.50	
w_{i12}(kJ/kg)	34.67	31.56	28.67	25.78	23.33	20.11	
w_{o23}(kJ/kg)	101.98	101.33	99.95	99.23	98.41	97.61	
w_{o41}(kJ/kg)	77.94	78.03	79.02	80.01	79.11	79.65	
RW(%)	76.43	77.01	79.06	80.63	80.38	81.60	
w_n= w_{o23}+w_{o41}-w_{i12}	145.25	147.81	150.31	153.46	154.19	157.14	1860.49
η_th/PU	64.40	64.64	64.89	65.41	64.99	65.32	63.84
V_{reserv}(m3/kg)/PU)	0.6167	0.5655	0.5144	0.4633	0.4122	0.3611	8.68
V_{tot} (m3/kg)/PU)	0.6527	0.6010	0.5494	0.4978	0.4461	0.3944	9.16
$\Delta V_{\_act}$(m^3)	0.0360	0.0354	0.0350	0.0345	0.0339	0.0334	0.47
p_{ref}(bar)/PU	20.00	20.00	20.00	20.00	20.00	20.00	
Δp (bar)/(PU-cycle)	1.49	1.64	1.83	2.05	2.33	2.69	
qi_feedback (PU1)=h_3-h_5(kJ/kg-cycle							340.70
Useful output work=$\sum w_n$ (kJ/kg-cycle)							1519.79

2.7.2 SSPM composed by 9 PUs operating with a PGT-sVsVs thermal cycle with helium and T_D: 75 K

Table 5: Processed data for a SSPM composed by 9 cascaded PUs into the temperature range of 1000-350 K.

sp	T(K)	p(bar)	v(m^3/kg)	u(kJ/kg)	h(kJ/kg)	s(kJ/kg. K)
			PU 1; TD = 75 K			
1	925.00	20.00	0.9632	2888.30	4814.70	27.633
2	934.14	20.50	0.9490	2916.90	4867.59	27.633
3	1000.00	21.94	0.9490	3122.20	5204.70	27.845
4	963.51	20.00	1.0031	3008.30	5033.61	27.845
5	900.10	18.69	1.0031	2810.70	4685.00	27.633
			PU 2; TD = 75 K			
1	850.00	20.00	0.8853	2654.60	4425.30	27.194
2	858.40	20.50	0.8723	2680.90	4473.86	27.194
3	925.00	22.09	0.8723	2888.50	4815.30	27.427
4	888.98	20.00	0.9258	2776.10	4646.46	27.427
5	825.00	18.56	0.9258	2576.70	4295.00	27.194
			PU 3; TD = 75 K			
1	775.00	20.00	0.8075	2420.90	4035.90	26.715

2	782.75	20.50	0.7957	2445.10	4080.79	26.715
3	850.00	22.26	0.7957	2654.80	4426.00	26.972
4	814.39	20.00	0.8484	2543.70	4258.96	26.972
5	750.00	18.42	7500.8484	2342.90	3905.60	26.715
			PU 4; TD = 75 K			
1	700.00	20.00	0.7296	2187.20	3646.50	26.186
2	706.93	20.50	0.7189	2208.80	3686.61	26.186
3	775.00	22.47	0.7189	2421.10	4036.60	26.473
4	739.77	20.00	0.7709	2311.10	3871.27	26.473
5	674.80	18.25	0.7709	2108.60	3515.10	26.186
			PU 5; TD = 75 K			
1	625.00	20.00	0.6518	1953.50	3257.10	25.598
2	631.23	20.50	0.6423	1973.00	3293.21	25.598
3	700.00	22.73	0.6423	2187.40	3647.30	25.921
4	665.15	20.00	0.6935	2078.60	3483.68	25.921
5	599.70	18.03	0.6935	1874.60	3125.10	25.598
			PU 6; TD = 75 K			
1	550.00	20.00	0.5740	1719.80	2867.70	24.934
2	555.45	20.50	0.5655	1736.80	2899.26	24.934
3	625.00	23.07	0.5655	1953.70	3258.00	25.302
4	590.40	20.00	0.6159	1845.70	3095.46	25.302
5	524.70	17.78	0.6159	1640.80	2735.60	24.934
			PU 7; TD = 75 K			
1	475.00	20.00	0.496120	1486.00	2478.30	24.173
2	479.73	20.50	0.488870	1500.80	2505.74	24.173
3	550.00	23.50	0.488870	1719.90	2868.80	24.599
4	515.63	20.00	0.5383	1612.70	2707.16	24.599
5	475.00	20.00	0.496120	1486.00	2478.30	24.173
			PU 8; TD = 75 K			
1	400.00	20.00	0.4183	1252.20	2088.80	23.281
2	404.00	20.50	0.4122	1264.70	2112.13	23.281
3	475.00	24.10	0.4122	1486.20	2479.60	23.786
4	440.90	20.00	0.4607	1379.70	2319.04	23.786
5	400.00	20.00	0.4183	1252.20	2088.80	23.281
			PU 9; TD = 75K			
1	325.00	20.00	0.3405	1018.40	1699.40	22.202
2	328.21	20.50	0.3355	1028.40	1718.07	22.202
3	400.00	24.98	0.3355	1252.40	2090.50	22.819
4	365.98	20.00	0.3830	1146.20	1930.03	22.819

5	300.30	16.41	0.3830	941.26	1569.90	22.202

Table 6: Results of the cascaded PUs from data processed in Table 5

PU	1	2	3	4	5	6	7	8	9	Total
LF(%)	0.90	0.90	0.90	0.90	0.90	0.90	0.90	0.90	0.90	0.90
Is_eff(%)	0.90	0.90	0.90	0.90	0.90	0.90	0.90	0.90	0.90	0.90
T_3_sVsVs	1000.00	925.00	850.00	775.00	700.00	625.00	550.00	475.00	400.00	
T_1_sVsVs	925.00	850.00	775.00	700.00	625.00	555.45	475.00	400.00	325.00	
qi_(h_3-h_2)/PU(kJ/kg)	337.11	341.44	345.21	349.99	354.09	358.74	363.06	367.47	372.43	2449.64
q_{o_34}(kJ/kg)	348.61	351.46	353.36	356.17	358.58	359.86	360.56	361.04	360.13	2488.60
$q_{\_rec}$(kJ/kg)	348.61	351.46	353.36	356.17	358.58	359.86	360.56	361.04	360.13	2015.77
mean_rec_T(K)	944.26	869.49	794.70	719.89	645.08	570.20	495.32	420.45	345.49	
w_{i12}(kJ/kg)	52.89	48.56	44.89	40.11	36.11	31.56	27.44	23.33	18.67	
w_{o23}(kJ/kg)	153.98	151.96	150.34	148.80	147.26	146.29	145.48	144.50	144.42	
w_{o41}(kJ/kg)	116.73	117.27	117.27	118.26	118.80	118.89	118.53	117.72	116.55	
RW(%)	75.81	77.17	78.01	79.48	80.67	81.27	81.48	81.46	80.70	
w_n= w_{o23}+w_{o41}-w_{i12}	217.82	220.67	222.72	226.95	229.95	233.62	236.56	238.89	242.31	1588.28
η_th/PU	64.61	64.63	64.52	64.84	64.94	65.12	65.16	65.01	65.06	64.88
V_{reserv}(m3/kg)/PU)	0.9490	0.8723	0.7957	0.7189	0.6423	0.5655	0.4889	0.4122	0.3355	5.03
V_{tot} (m3/kg)/PU)	1.0031	0.9258	0.8484	0.7709	0.6935	0.6159	0.5383	0.4607	0.3830	5.40
$\Delta V_{\_act}$(m^3)	0.0541	0.0535	0.0527	0.0520	0.0512	0.0503	0.0494	0.0485	0.0475	0.36
p_{ref}(bar)/PU	20.00	20.00	20.00	20.00	20.00	20.00	20.00	20.00	20.00	
Δp (bar)/(PU-cycle)	1.44	1.59	1.76	1.97	2.23	2.57	3.00	3.60	4.48	
qi_feedback (PU1)=h_3-h_5(kJ/kg-cycle										519.70
Useful output work=∑ w_n (kJ/kg-cycle)										1588.28

2.7.3 SSPM composed by 7 PUs operating with a PGT-sVsVs thermal cycle with helium and T_D: 100 K

Table 7: Processed data for a SSPM composed by 7 cascaded PUs into the temperature range of 1000-350 K.

sp	T(K)	p(bar)	v(m^3/kg)	u(kJ/kg)	h(kJ/kg)	s(kJ/kg. K)
			PU 1; TD = 100 K			
1	900.00	20.00	0.9372	2810.40	4684.90	27.491
2	908.94	20.50	0.9235	2995.80	4736.57	27.491
3	1000.00	22.55	0.9235	3122.20	5204.80	27.789
4	953.17	20.00	0.9924	2976.10	4985.38	27.789
5	866.00	18.17	0.9924	2704.40	4507.80	27.491
			PU 2; TD = 100 K			
1	800.00	20.00	0.8334	2498.80	4165.70	26.879
2	807.87	20.50	0.8211	2523.40	4211.26	26.879
3	900.00	22.84	0.8211	2810.60	4685.70	27.216
4	853.58	20.00	0.8890	2665.80	4468.08	27.216

5	766.00	17.95	0.8890	2392.80	3988.50	26.879
			PU 3; TD = 100 K			
1	700.00	20.00	0.7296	2187.20	3646.50	26.186
2	908.94	20.50	0.7189	2208.80	3686.61	26.186
3	800.00	23.20	0.7189	2499.00	4166.60	26.572
4	754.01	20.00	0.7857	2355.50	3950.87	26.572
5	666.20	17.67	0.7857	2081.80	3470.30	26.186
			PU 4; TD = 100 K			
1	600.00	20.00	0.6258	1875.60	3127.30	25.386
2	908.94	20.50	0.6167	1894.20	3161.97	25.386
3	700.00	23.68	0.6167	2187.40	3647.60	25.836
4	654.35	20.00	0.6823	2045.00	3433.31	25.836
5	566.30	17.31	0.6823	1770.40	2951.40	25.386
			PU 5; TD = 100 K			
1	500.00	20.00	0.5221	1563.90	2608.10	24.439
2	504.94	20.50	0.5144	1579.40	2636.77	24.439
3	600.00	24.36	0.5144	1875.80	3128.60	24.977
4	554.57	20.00	0.5787	1734.00	2915.12	24.977
5	466.70	16.83	0.5787	1460.00	2434.10	24.439
			PU 6; TD = 100 K			
1	400.00	20.00	0.4183	1252.20	2088.80	23.281
2	404.00	20.50	0.4122	1264.70	2112.13	23.281
3	500.00	25.37	0.4122	1564.20	2609.80	23.946
4	454.70	20.00	0.4751	1422.70	2396.50	23.946
5	367.40	16.16	0.4751	1150.50	1918.30	23.281
			PU 7; TD = 100 K			
1	300.00	20.00	0.314540	940.44	1569.50	21.787
2	303.00	20.50	0.309980	949.82	1587.06	21.787
3	400.00	27.05	0.309980	1252.50	2091.10	22.654
4	354.54	20.00	0.3711	1110.50	1876.63	22.654
5	268.50	15.15	0.3711	842.06	1404.30	21.787

Table 8: Results the cascaded PUs from data processed in Table 7

PU	1	2	3	4	5	6	7	Total
LF(%)	0.90	0.90	0.90	0.90	0.90	0.90	0.90	0.90
Is_eff(%)	0.90	0.90	0.90	0.90	0.90	0.90	0.90	0.90
T_3_sVsVs	1000.00	900.00	800.00	700.00	600.00	500.00	400.00	
T_1_sVsVs	900.00	800.00	700.00	600.00	500.00	404.00	300.00	
qi_(h_3-h_2)/PU(kJ/kg)	468.23	474.44	479.99	485.63	491.83	497.67	504.04	3401.84
q_{o_34}(kJ/kg)	477.58	479.58	480.57	481.91	481.02	478.20	472.33	3351.19

q_{-rec}(kJ/kg)	477.58	479.58	480.57	481.91	481.02	478.20	472.33	0.00
mean_rec_T(K)	926.59	826.79	350.36	627.18	527.29	427.35	327.27	
w_{i12}(kJ/kg)	51.67	45.56	40.11	34.67	28.67	23.33	17.56	
w_{o23}(kJ/kg)	197.48	195.86	194.16	192.86	192.13	191.97	193.02	
w_{o41}(kJ/kg)	159.39	159.48	158.58	158.31	156.60	153.45	148.68	
RW(%)	80.71	81.43	81.68	82.09	81.51	79.93	77.03	
$w_n = w_{o23}+w_{o41}-w_{i12}$	305.20	309.78	312.63	316.50	320.07	322.09	324.15	2210.41
η_th/PU	65.18	65.29	65.13	65.17	65.08	64.72	64.31	
V_{reserv}(m3/kg)/PU)	0.9235	0.8211	0.7189	0.6167	0.5144	0.4122	0.3100	4.32
V_{tot} (m3/kg)/PU)	0.9924	0.8890	0.7857	0.6823	0.5787	0.4751	0.3711	4.77
$\Delta V_{\_act}(m^3)$	0.0689	0.0679	0.0668	0.0656	0.0643	0.0628	0.0612	0.4575
p_{ref}(bar)/PU	20.00	20.00	20.00	20.00	20.00	20.00	20.00	
Δp (bar)/(PU-cycle)	2.05	2.34	2.70	3.18	3.86	4.87	6.55	
qi_feedback (PU1)=h_3-h_5(kJ/kg-cycle								697.00
Useful output work=$\sum w_n$ (kJ/kg-cycle)								1513.41

2.7.4 SSPM composed by 4 PUs operating with a PGT-sVsVs thermal cycle with helium and T_D: 150 K

Table 9: Processed data for a SSPM composed by 4 cascaded PUs into the temperature range of 1000-350 K.

sp	T(K)	p(bar)	v(m^3/kg)	u(kJ/kg)	h(kJ/kg)	s(kJ/kg. K)
			PU 1; TD = 150 K			
1	850.00	20.00	0.8853	2654.60	4425.30	27.194
2	858.40	20.50	0.8723	2680.90	4473.86	27.194
3	1000.00	23.88	0.8723	3122.30	5205.20	27.670
4	931.58	20.00	0.9700	2908.80	4884.44	27.670
5	799.70	17.17	0.9700	2497.80	4163.30	27.194
			PU 2; TD = 150 K			
1	700.00	20.00	0.7296	2187.20	3646.50	26.186
2	706.93	20.50	0.7189	2208.80	3686.61	26.186
3	850.00	24.65	0.7189	2654.90	4426.70	26.761
4	781.96	20.00	0.8147	2442.60	4107.47	26.761
5	650.20	16.63	0.8147	2031.90	3386.90	26.186
			PU 3; TD = 150 K			
1	550.00	20.00	0.5740	1719.80	2867.70	24.934
2	555.45	20.50	0.5655	1736.80	2899.26	24.934
3	700.00	25.83	0.5655	2187.50	3648.30	25.655
4	631.93	20.00	0.6590	1975.10	3328.62	25.655
5	501.50	15.87	0.6590	1568.40	2614.50	24.934
			PU 4; TD = 150 K			
1	400.00	20.00	0.4183	1252.20	2088.80	23.281
2	404.00	20.50	0.4122	1264.70	2112.13	23.281
3	550.00	27.90	0.4122	1720.20	2870.20	24.243
4	481.46	20.00	0.5028	1506.20	2547.64	24.243

5	353.70	14.38	0.5028	1107.70	1846.70	23.281

Table 10: Results the cascaded PUs from data processed in Table 9

PU	1	2	3	4	Total
LF(%)	0.90	0.90	0.90	0.90	0.90
Is_eff(%)	0.90	0.90	0.90	0.90	0.90
T_{3}_sVsVs	1000.00	850.00	700.00	550.00	
T_{1}_sVsVs	850.00	700.00	550.00	400.00	
qi_(h_3-h_2)/PU(kJ/kg)	731.34	740.09	749.04	758.07	1908.30
q_{o_34}(kJ/kg)	721.14	720.57	714.12	700.94	1919.64
$q_{\_rec}$(kJ/kg)	721.14	720.57	714.12	700.94	1554.91
mean_rec_T(K)	890.79	740.98	275.28	440.73	
w_{i12}(kJ/kg)	48.56	40.11	31.56	23.33	
w_{o23}(kJ/kg)	288.68	287.31	287.71	290.30	
w_{o41}(kJ/kg)	235.80	233.64	227.88	217.89	
RW(%)	81.68	81.32	79.20	75.06	
w_n= w_{o23}+w_{o41}-w_{i12}	475.93	480.84	484.04	484.86	1925.66
η_th/PU	65.08	64.97	64.62	63.96	
V_{reserv}(m3/kg)/PU)	0.8723	0.7189	0.5655	0.4122	0.00
V_{tot} (m3/kg)/PU)	0.9700	0.8147	0.6590	0.5028	0.00
$\Delta V_{\_act}$(m^3)	0.0977	0.0958	0.0934	0.0906	0.3775
p_{ref}(bar)/PU	20.00	20.00	20.00	20.00	
Δp (bar)/(PU-cycle)	3.38	4.15	5.33	7.40	
qi_feedback (PU1)=h_3-h_5(kJ/kg-cycle					1041.90
Useful output work=∑ w_n (kJ/kg-cycle)					883.76

2.7.5 Comparison of results for the analysis of four studied cases SSPMs

Table 11 illustrates the main results (most relevant data) of the four studied cases. Based on the interdependence between critical and common parameters in the cases studied, which are relevant for key analyses and conclusions on prototype design, let's consider the following parameters useful for analyzing table 11 focused on analysis and comparisons:

Table 11: Comparison of the results derived from processing cycle's data for all studied cases

	SSPM results			
	Case 1	Case 2	Case 3	Case 4
NPUs/SSPM: number of PUs/SSPM	13	9	7	4
T_D (K): constant temperature drop	50	75	100	150
LF (%): mechanical and thermal losses	0.9	0.9	0.9	0,9
Is_eff (%): isentropic efficiency	0.9	0.9	0.9	0.9
q_{i23}/SSPM(kJ/kg): total heat inlet/SSPM	2897.92	3189,54	3401.84	2978.54
q_{o45}(kJ/kg): total heat output/SSPM	3001.60	3209,77	3351.19	2856.77
q_rec(kJ/kg): heat recovered /SSPM	2431.17	2599,91	2714.46	2313.98
w_{i12}(kJ/kg): input feed pump work	484,78	323.56	241,56	143.56
W_{o34}(kJ/kg): expansion output useful work/SSPM	1344,20	1233,02	1357.48	1154.00
W_{o51}(kJ/kg) contraction output useful work/SSPM	1001,07	1006,02	1094.49	915.21
RW: average ratio of contraction to expansion work	74,65	79,56	80.62	79.32
w/PU/cy(kJ/kg)=∑w/SSPM: total useful work/SSPM	1860.49	2069.48	2210.41	1925.66

η_{th}/SSPM. Average thermal efficiency /SSPM	63.84	64.88	64.98	64.66
V_{reserv}(m^3/kg)/PU): Reservoir volume /SSPM	8.68	5.03	4.32	2.57
V_{tot} (m^3/kg)/PU): Total working volume/SSPM	9.16	5.40	4.77	2.95
ΔV_act(m^3)= Vtot-Vreserv: actuator volume	0.470	0.460	0.458	0.378
p_{ref}(bar)/PU: pressure initial in each cycle	20	20	20	20
qi_feedback(PU1)=h_3-h_5(kJ/kg-cycle)	340.70	519.70	697.00	1041.90
Net mechanical work/SSPM (kJ/kg-cycle): output useful work/SSPM	1519.79	1549,78	1513.41	883.76

Among all interesting data of the Table 11, the useful work per cycle (profit without propellant costs) is essential. Therefore, Fig. 6 illustrates total output work delivered by each SSPM, feedback added heat and net output useful work as function of the constant temperature drop in each PU of every SSPM. To identify the curves in the Fig. 6, take into account that black line represent total work due to SSPM PUs as function of temperature drop (T_D) or (T_{drop}) in each studied SSPM; red line represents useful work due to the SSPM, and pink line represent feedback heat responsible for driving the SSPM.

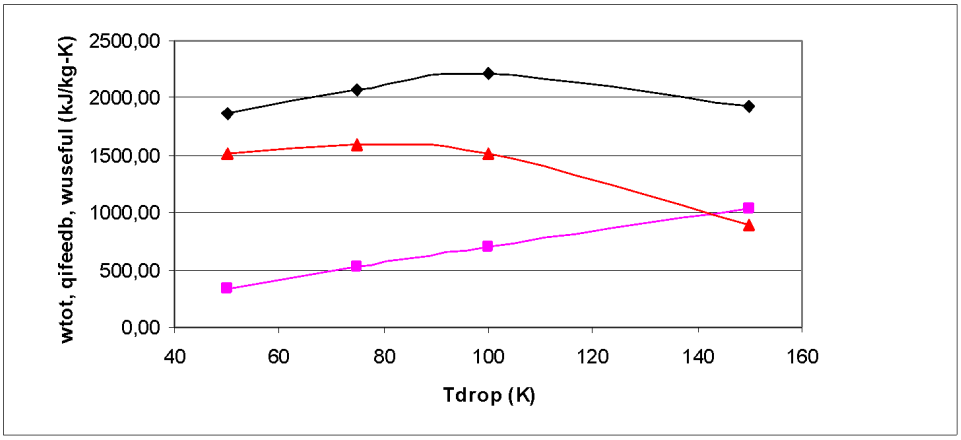

Figure 6: Illustration of the total output work, feedback added heat and net output useful work as function of the constant temperature drop in each PU of the SSPM

Looking at Figure 6, it can be seen that the black curve (total useful mechanical work due to the PU cascade) exhibits its maximum value for a temperature difference between each PU of 100 K, which requires 7 PUs to complete the corresponding SSPM, while the red curve (net useful mechanical work due to the PU cascade) exhibits its maximum value for a temperature difference between each PU of 75 K, which requires 9 PUs to complete the SSPM.

Given that the number of PUs in each Self-Sustaining Power Machine (SSPM) influences the manufacturing and maintenance costs, as well as the free power supplied and therefore the profits, it is worth noting that this observation reveals a functional relationship between the number of PUs, temperature droop, and profits, which can be estimated by solving a simple problem that consists of minimizing a cost function based on the parameters handled.

Table 12: Illustration of the influence of the feedback heat on the output useful net free work as function of the number of PUs whish is a function of the temperature drop not depicted in the table.

Table 12: Illustration of case studies 2 and 3 to analyze the power scaling methodology.

Case studies considered	Case1	Case2	Case3	Case4
NPU /SSPM	13	9	7	4
Feedback Heat (kJ/kg)	340,7	519,7	697	1041,9
Free self-sustained useful work (kJ/kg)	1519,79	1549,28	1513,41	883,76
Thermal V(m^3)/SSPM	9,16	5,4	4,77	2,95
T_D (K)/PU	50	75	100	150

The data depicted in Table 12 is graphically illustrated with Fig. 7 to show the influence of the feedback heat on the output useful net free work as function of the number of PUs whish is a function of the temperature drop not depicted in the figure. Although the self-sustaining work in case study 3 is somewhat lower than the maximum value (which is due to case 2), case 3 may be more advantageous because it uses fewer PUs than case 2. That is, 7 PUs in case 3 instead of 9 PUs in case 2).

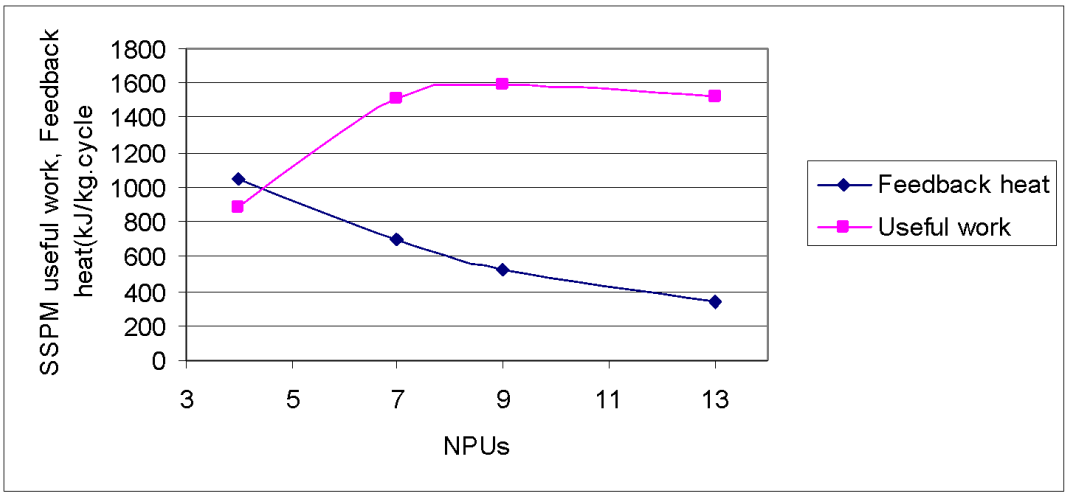

Figure 7: Illustration of the influence of the feedback heat in the total output free net work as function of the number of cascaded PUs of an SSPM

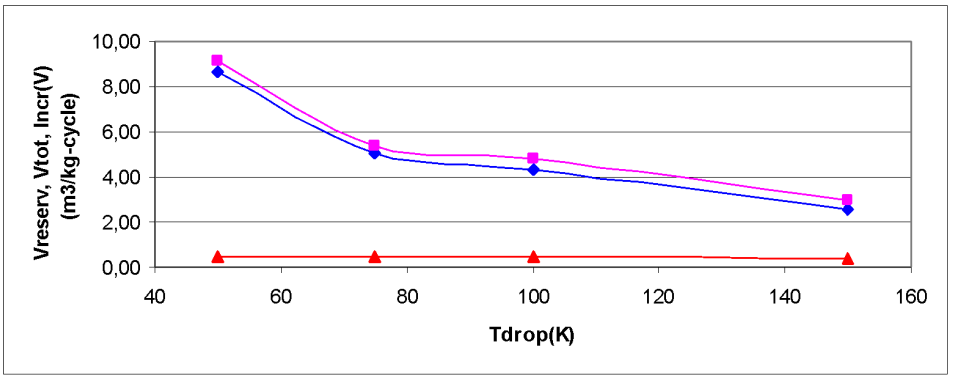

Figure 8: Illustration of the evolution of the total thermodynamic volumes of the SSPMs under study as a function of the temperature jump and/or number of PUs of each SSPM

Fig. 8 shows the evolution of the total thermodynamic volumes of the SSPMs under study as a function of the temperature difference and/or number of SSPM-based PUs in each SSPM. Thermodynamic volume is important for estimating the space occupied by each SSPM, but also as data for estimating the weight associated with the reservoirs responsible for a high proportion of the volume of each SSPM.

2.7.6 Scaling SSPM dimensions too meet power demand in space applications

To meet the energy demands of space applications, it is necessary to satisfy the needs of the following essential services:

-- Energy support for local resource exploitation services, including the most plausible emergencies.

-- Interplanetary transport to/from local orbit, and

-- Transport resources in orbit (spare propulsion system and propellant), and

These requirements consists of the necessary dry and wet masses due to total energy demands, which include supplying specific work under demand and structural mass and volume of the TWF reservoirs and propellant reservoirs.

By scaling proportionally the reservoirs volume of the TWF of the SSPM, which undergoes scaling the mass of this fluid, it is obtained the actual power demand considering mass flow rate (**mfr**) accordingly.

Ideal power is usually estimated from the specific work (the corresponding input or output work done per unit time) of one kg of TWF per second (s). That is, the product of the mfr of TWF and the specific work.

$$P = Power = \dot{m}_p \cdot w\,[(kg/s)\cdot(kJ/kg)] \rightarrow (kJ/s) \rightarrow kW \quad (14)$$

Although the self-sustaining work in case study 3 is somewhat lower than the maximum value (which is due to case 2), case 3 may be more advantageous because it uses fewer PUs than case 2. That is, 7 PUs in case 3 instead of 9 PUs in case 2 according to Table 13. This simple strategy may influence positively the manufacturing and maintenance efforts. Table 13 illustrates the fundamental data for proceeding with the escalation of cases 2 and 3.

Table 13: Dimensional scaling of SSPM-based plants considering two previously studied cases

Cases considered	Case2	Case3
NPU	9	7
Feedback heat (kJ/kg)	519,7	697
work/cycle (kJ/kg)	1549,28	1513,41
Thermal V(m^3)/SSPM	5,4	4,77
T_D (K)/PU	75	100

Table 14: Meeting the power demand by scaling the thermodynamic volume of a given SSPM associated with the specific work and mass flow rate.

The data in Table 14 are interpreted such that, with reference to case 2, for a TWF flow rate of 1 kg/s and a cycle time of 1 second, a thermodynamic volume of 5.4 m^3 is required to obtain 1.549 MW of power. Likewise, for a TWF flow rate of 10 kg/s and a cycle time of 1 second, a thermodynamic volume of 54 m^3 is required to obtain 15.49 MW of power. The data in Table 15 are interpreted in the same way as in Table 14.

Table 14: Dimensional scaling results of SSPM plants considering t2e case study 2

Case 2; mfr_SSPM(kg/s) for a cycle(s): **1;** Total Thermal Volume = mfr*V_SSPM (m^3): **5,4**						
Cycle time/PU (s)	1	2	5	10	15	20
mfr_SSPM(kg/s-cycle)	1,00	0,50	0,20	0,10	0,07	0,05
P=mfr*w(MW)	**1,54928**	**0,77**	**0,31**	**0,15**	**0,10**	**0,08**
Case 2; mfr_SSPM(kg/s) for a cycle(s): **10;** Total Thermal Volume = mfr*V_SSPM (m^3): **54**						
Cycle time/PU (s)	1	2	5	10	15	20
mfr_SSPM(kg/s-cycle)	10,00	5,00	2,00	1,00	0,67	0,50
P(MW)	**15,4928**	**7,75**	**3,10**	**1,55**	**1,03**	**0,77**
Case 2; mfr_SSPM(kg/s) for a cycle(s): **50;** Total Thermal Volume = mfr*V_SSPM (m^3): **270**						
Cycle time/PU (s)	1	2	5	10	15	20
mfr_SSPM(kg/s-cycle)	50,00	25,00	10,00	5,00	3,33	2,50
P(MW)	**77,464**	**38,73**	**15,49**	**7,75**	**5,16**	**3,87**
Case 2;mfr_SSPM(kg/s) for a cycle(s): **100;** Total Thermal Volume = mfr*V_SSPM (m^3): **540**						
Cycle time/PU (s)	1	2	5	10	15	20
mfr_SSPM(kg/s-cycle)	100,00	50,00	20,00	10,00	6,67	5,00
P=mfr*w/1000(MW)	**154,928**	**77,46**	**30,99**	**15,49**	**10,33**	**7,75**
Case 2; mfr_SSPM(kg/s) for a cycle(s): **200;** Total Thermal Volume = mfr*V_SSPM (m^3): **1080**						
Cycle time/PU (s)	1	2	5	10	15	20
mfr_SSPM(kg/s-cycle)	200,00	100,00	40,00	20,00	13,33	10,00
P(MW)	**309,856**	**154,93**	**61,97**	**30,99**	**20,66**	**15,49**
Case 2; mfr_SSPM(kg/s) for a cycle(s): **500;** Total Thermal Volume = mfr*V_SSPM (m^3): **2700**						
Cycle time/PU (s)	1	2	5	10	15	20
mfr_SSPM(kg/s-cycle)	500,00	250,00	100,00	50,00	33,33	25,00

P(MW)	**774,64**	**387,32**	**154,93**	**77,46**	**51,64**	**38,73**

Table 15: Dimensional scaling results of SSPM plants considering te case study 3

Case 3; mfr_SSPM(kg/s) for a cycle(s): **1;** Total Thermal Volume = mfr*V_SSPM (m^3): **4,77**						
Cycle time/PU (s)	1	2	5	10	15	20
mfr_SSPM(kg/s-cycle)	1,00	0,50	0,20	0,10	0,07	0,05
P(MW)	**1,51341**	**0,76**	**0,30**	**0,15**	**0,10**	**0,08**
Case 3;mfr_SSPM(kg/s) for a cycle(s): **10;** Total Thermal Volume = mfr*V_ SSPM (m^3): **47,7**						
Cycle time/PU (s)	1	2	5	10	15	20
mfr_SSPM(kg/s-cycle)	10,00	5,00	2,00	1,00	0,67	0,50
P(MW)	**15,1341**	**7,57**	**3,03**	**1,51**	**1,01**	**0,76**
Case 3;mfr_SSPM(kg/s) for a cycle(s): **50;** Total Thermal Volume = mfr*V_SSPM (m^3): **238,5**						
Cycle time/PU (s)	1	2	5	10	15	20
mfr_SSPM(kg/s-cycle)	50,00	25,00	10,00	5,00	3,33	2,50
P(MW)	**75,6705**	**37,84**	**15,13**	**7,57**	**5,04**	**3,78**
Case 3;mfr_SSPM(kg/s) for a cycle(s): **100;** Total Thermal Volume = mfr*V_SSPM (m^3): **477**						
Cycle time/PU (s)	1	2	5	10	15	20
mfr_SSPM(kg/s-cycle)	100,00	50,00	20,00	10,00	6,67	5,00
P(MW)	**151,341**	**75,67**	**30,27**	**15,13**	**10,09**	**7,57**
Case 3; mfr_SSPM(kg/s) for a cycle(s): **200;** Total Thermal Volume = mfr*V_SSPM (m^3): **954**						
Cycle time/PU (s)	1	2	5	10	15	20
mfr_SSPM(kg/s-cycle)	200,00	100,00	40,00	20,00	13,33	10,00
P(MW)	**302,682**	**151,34**	**60,54**	**30,27**	**20,18**	**15,13**
Case 3;mfr_SSPM(kg/s) for a cycle(s): **500;** Total Thermal Volume= mfr*V_SSPM (m^3): **2385**						
Cycle time/PU (s)	1	2	5	10	15	20
mfr_SSPM(kg/s-cycle)	500,00	250,00	100,00	50,00	33,33	25,00
P(MW)	**756,705**	**378,35**	**151,34**	**75,67**	**50,45**	**37,84**

Once the total energy demand is known, dimensional scaling is carried out, which estimates, among other data, the total thermodynamic volume, which allows for an approximate estimate of the total mass of the spacecraft.

The following section deals briefly with the intensive energy consumption that requires two resources: non-recoverable propellant and intensive electricity generation: interplanetary propulsion associated with the transport inherent in resource exploitation.

3. Modelling of the Spacecraft Propulsion System.:

The analysis of jet propulsion is based on the principle of conservation of linear momentum, according to Newton's third law. The objective of the modeling task is to determine the actual electrical power demand to satisfy two basic needs:

-- Sufficient propulsive thrust (requiring significant quantities of non-recoverable propellant) and,

-- Electrical power to meet the total demand of resource exploitation tasks.

The propulsion thrust requirement is determined by the amount of propellant fluid available. The goal is to achieve a flight of a spacecraft at a speed that allows it to reach a desired location (satellite, artificial satellite planet, or resource storage or repropellanting platform in space orbit or geostationary position). Therefore, the consumption of propellant to reach a demanded velocity is critical.

3.1 Rocket Thrust

Thrust is the force that propels a rocket through the air. It is generated by a rocket engine as a result of accelerating a pressurized mass of gas. When the gas is expelled backward, the rocket is pushed forward in the

opposite direction—this is (action force equals reaction force) a direct application of Newton's third law of motion. Therefore we can think of the propulsion system as a machine designed to accelerate gas and produce thrust. The relationship between thrust, propellant mass flow rate, and required power depends on the thrust and power, where:

-- Thrust is directly proportional to the mass flow rate of the propellant, while

-- The power required is proportional to the mass flow rate multiplied by the kinetic energy imparted to the propellant fluid.

Since the mass flow rate ($\dot{m}$) is implied in both (thrust and power statements), let's describe thrust forces under a more detailed explanation.

3.1.1 Thrust Equation

The thrust force (F) from a jet engine, rocket, or propeller obeys Newton's second law. Therefore, considering ideal conditions follows that

$F = m \cdot a$, which is described as

$$F = \dot{m}_P \cdot v_e + A_e \cdot (p_e - p_a) \tag{15}$$

Where the notation in Eq. (15) is:

$\dot{m}_P$ ·	propellant fluid mass flow rate (kg/s).
v_e	propellant output velocity of the fluid (m/s)
A_e	exit area of the nozzle (m^2).
p_e	exhaust pressure (Pa).
p_a	ambient pressure (Pa).

For the simplest case of propulsion force such a rocket in a vacuum where propellant is completely expanded in a nozzle, the equation simplifies to:

$$F = \dot{m}_P \cdot v_e \text{ , since } A_e \cdot (p_e - p_a) = 0 \tag{16}$$

Eq (16) shows a direct linear relationship between mass flow rate and exhaust velocity.

3.1.2 Required Power

Power, can be defined as the rate of doing work, or the rate at which energy (kinetic energy or work) is transferred to the propellant fluid. Therefore, kinetic power P_K is the actual power contained in the exhaust propellant jet under ideal conductions. It consists of the kinetic energy imparted to the fluid per second (ideal jet power).

$$P_K = \frac{1}{2} \dot{m}_P \cdot v_e^{\,2} \tag{17}$$

The Input Power (P_{in}) is the required power that must be supplied to the engine from a power supply device. Due to the inherent irreversibilities mechanical power is always ***higher*** than the kinetic power due to inefficiencies which include friction, heat loss etc. The efficiency that relates power required with kinetic energy is called the propulsive efficiency (η_P). Therefore, the required power or input power is related with propulsive efficiency according to the Eq. (16)

$$P_{IN} \approx \frac{P_K}{\eta_P} = \frac{\frac{1}{2} \dot{m}_P \cdot v_e^{\,2}}{\eta_P} \tag{18}$$

The required power is proportional to the mass flow rate and to the square of the exhaust velocity. Nevertheless due to the inherent losses required power must be however. The input power has to be considerably higher than the kinetic power due to propulsive efficiency. To resolve this dilemma, a criterion is established: to achieve the

maximum steady state speed with a given amount of propellant fluid: High specific impulse (I_{SP}) is necessary as concluded in section (3.3.2).

3.1.3 Critical balance between thrust and energy efficiency

Let's combine the two boxed equations to see the crucial trade-off.

a) From the thrust equation (16):

$$v_e = \frac{F}{\dot{m}_P} \tag{19}$$

b) Substituting (19) into power Eq. (17) yields:

$$P_K = \frac{1}{2}\dot{m}_P \cdot \left(\frac{F}{\dot{m}_P}\right)^2 = \frac{1}{2}\cdot\frac{F^2}{\dot{m}_P} \tag{20}$$

The meaning of Eq. (20) suggest us an important insight: For a constant thrust force (F), the required power (P_K) is inversely proportional to the mass flow rate ($\dot{m}_P$). This suggests that a higher propellant mass flow rate requires less power. However, propellant is not recoverable and is therefore depleted more quickly as available power is applied. Conclusions about this topic will be shown in section 3.3.2.

3.2 Propulsion thrust formulation based on an ideal thermo-mechanical model:

It is assumed that the propellant fluid flow obeys an ideal isentropic and adiabatic expansion process without friction at the nozzle if its math-model is restricted to the absence of losses. Therefore, the balance under assumed conditions can be approached as the balance between the drop in enthalpy (***Δh***) along the nozzle and the increment in kinetic energy (E_k) which can be described in Eq. (21) as:

$$\Delta E_k k = \Delta h \tag{21}$$

Assuming ΔE_k as the change in kinetic energy and Δh is the change in enthalpy.

Eq. (21) can be explicitly represented as

$$\frac{V_e^{\,2} - V_i^{\,2}}{2} = \Delta h = h_i - h_e \tag{22}$$

From Eq. (4) it is obtained the exit velocity of the propellant as

$$V_e^{\,2} = V_i^{\,2} + 2\cdot(h_i - h_e) \quad and \quad V_e = \sqrt{V_i^{\,2} + 2\cdot(h_i - h_e)} \tag{23}$$

Assuming that the velocity of propellant v_p = $\boldsymbol{V_i}$ at the nozzle input has a negligible value with respect to the exit velocity v_p = $\mathbf{V_e}$, and all losses neglected, from Eq. (14) follows that

$$V_e^{\,2} \approx 2\cdot\Delta h = 2\cdot(h_i - h_e) \quad \text{and finally,}$$

$$V_e \approx \sqrt{2\cdot\Delta h} = \sqrt{2\cdot(h_i - h_e)} \tag{24}$$

Then from Eq. (16) the propulsion thrust can also be expressed as

$F = \dot{m}_P \cdot V_e = \dot{m}_P \cdot \sqrt{V_i^{\,2} + 2\cdot(h_i - h_e)}$, or neglecting the initial kinetic energy then we obtain

$$F \approx \dot{m}_P \cdot \sqrt{2\cdot\Delta h)} = \dot{m}_P \cdot \sqrt{2\cdot(h_i - h_e)} \tag{25}$$

3.2.1 Power based on enthalpy change

Ideal power is usually estimated from the specific work (the corresponding input or output work done per unit time) of one kg of TWF during a second (s). That is, the product of the mass flow rate ($\dot{m}_p$ =mfr) of TWF and the specific work. When specific work is expressed by means of an enthalpy change, power is expressed as

$$P = Power = \dot{m}_p \cdot \Delta h\,[(kg/s)\cdot(kJ/kg)] \rightarrow (kJ/s) \rightarrow kW \tag{26}$$

The actual adiabatic expansion processes carried out in all nozzles exhibit inherent losses due to irreversibilities. Depending on the nozzle design profile and operating conditions, these losses can exceed 20%. However, in our approach, these losses are disregarded, and therefore the ideal case is considered.

The Input power (P_{in}) according Eq. (26), which means the required power to satisfy a given thrust under ideal conductions is the ratio of the specific thermodynamic work to the propulsion efficiency

$$P_{IN} \approx \frac{P}{\eta_P} = \frac{\dot{m}_P \cdot w}{\eta_P} = \frac{\dot{m}_P \cdot \Delta h}{\eta_P} \tag{27}$$

3.3 Total impulse (I) and specific Impulse (I_{sp}):

Since the total impulse of a dynamic body is a linear momentum and it is a conserved quantity, in this context, it is useful to relate it to the propulsion thrust force to obtain a benchmark of the propulsion dynamic conditions. Balancing impulse with linear momentum yields:

$$I = F \cdot \Delta t \rightarrow \int F \cdot dt = \int \dot{m} \cdot V_e \cdot dt = m \cdot V_e$$

$$I = m \cdot V_e \tag{28}$$

3.3.1 Specific Impulse (I_{sp}):

The specific impulse (Isp), expressed in seconds, is defined as the ratio of the total impulse to the total weight of the spacecraft (which includes the actual weight of the satellite (payload) plus the weight of the propellant and the structural weight), where $g_0 \approx 9.81$ is the standard acceleration due to gravity at sea level. It is a measure of the rocket engine's efficiency, representing the thrust produced per unit of propellant mass flow rate, that is, the amount of propellant expelled and consumed per second.

$$I_{sp} = \frac{I}{m \cdot g_0} = \frac{V_{eq}}{g_0} \tag{29}$$

which can also be expressed as

$$I_{sp} = \frac{F}{\dot{m} \cdot g_0} \tag{30}$$

A higher specific impulse means the engine is more propellant-efficient, which yields more thrust for the same amount of propellant. This concept is crucial for space exploration where propellant mass is a critical factor.

3.3.2 Relationship of specific impulse with thrust

(a) **Thrust vs. I_{sp}**: While a high specific impulse is good for propellant consumption efficiency, it's different from thrust, which is the raw force the engine produces.

(b) **High thrust, low I_{sp}**: A propulsion engine can have a high thrust but a low specific impulse if it has to consume a lot of propellant to achieve that thrust.

(c) **High I_{sp}, low thrust**: Conversely, an engine can have a high specific impulse and low thrust. This is common in engines like ion thrusters, which use a lot of energy to expel propellant at very high speeds, providing a small but highly efficient and long-lasting thrust.

(d) **Combined efficiency**: The most efficient rockets have a high specific impulse for the amount of thrust they produce, meaning they are both powerful and propellant-efficient.

3.4 The rocket dynamics approached by the Tsiolkovsky Equation

The goal is to achieve a previously unattainable cruising speed with a minimal amount of propellant. This milestone requires propellant temperatures and pressures that are currently problematic or even impossible.

The dynamics of rocket launches and landings are not included in this study; meaning that it deals with the dynamics between orbits and transits between accessible satellites or planets of the solar system.

The challenge lies in shortening travel time, which means saving propulsion resources that are technically difficult to obtain and costly.

Considering a jet-powered spacecraft, the Tsiolkovsky equation solves the problem of finding the terminal or resultant spacecraft velocity ($\mathbf{v_s}$)as a function of the propellant fluid velocity ($\mathbf{v_p}$,) and the ratio of the consumed mass of propellant fluid ($\mathbf{m_p}$) to the remaining mass of the spacecraft ($\mathbf{m_s}$), which includes the structure and the remaining propellant fluid, if any.

Table 15: Parameters associated with the spacecraft model

v_s	Spacecraft final velocity including steady state velocity (km/s)
v_p	Propellant velocity of the expelled propellant fluid (km/s)
m_p	mass of propellant fluid (gas)
m_s	mass of the spacecraft (satellite) without the expelled propellant
m_T=m_s+m_p	total aircraft mass including propellant
$\dot{m}_p$	Propellant mass flow rate
m_{pinit}	Initial mass of propellant fluid into the propellant reservoir
$\beta_{(h)}$	Drag losses (time-variant viscous friction coefficient) as function of atmospheric height and spacecraft velocity

The final result given as the spacecraft velocity (v_s) due to Tsiolkovsky development according to the notation depicted in Table 15 is:

$$\frac{v_s}{v_p} = \cdot \ln\left(\frac{m_s + m_p}{m_s}\right) = \ln\left(1 + \frac{m_p}{m_s}\right) \tag{31}$$

and finally,

$$\frac{v_s}{v_p} = \ln\left(1 + \frac{m_p}{m_s}\right) \tag{32}$$

Thus, in exponential form yields

$$1 + \frac{m_p}{m_s} = e^{(v_s / v_p)} \tag{33}$$

And consequently, the ratio of masses (propellant/spacecraft without propellant) yields finally the amount of required propellant fluid from (9) as:

$$\frac{m_p}{m_s} = e^{(v_s / v_p)} - 1 \tag{34}$$

Equations (29) and (31) are useful for estimating velocities as a function of masses, as well as for determining masses as a function of velocities. For example, from equation (34), the amount of propellant needed to change the desired velocity of a spacecraft to vf, given vo, is given as:

$$m_p = m_s \cdot (e^{(v_s / v_p)} - 1) \tag{35}$$

This exponential growth with speed makes it relevant to optimize the rocket's mass to reduce the propellant required. Therefore, rockets consist of phases, which are phased out as they become unnecessary.

3.4.1 An example of the procedure

To illustrate the usefulness of Tsiolkovsky's development without wasting time let's look at a procedural methodology through two simple examples:

a)--If it is desired to place a certain amount of payload m_s orbiting at a certain speed v_s, the amount of propellant fluid consumed or needed m_p is obtained by clearing m_p according to Eq. (35) as follows:

To do so it is assumed a m_s = **2000 kg** spaceship to be launched into low Earth orbit (LEO) by ejecting **hot gases at an exit velocity** v_p of **4 km/s**, how much propellant is required by the thruster to reach an escape velocity of the spacecraft of v_s = **12 km/s** ?

$$m_p = m_s \cdot (e^{(v_s / v_p)} - 1) = 2000\ kg \cdot (e^{(12/4)} - 1) \approx 38171\ kg \tag{36}$$

That's about **19 kg** of propellant for every kilogram of payload transported m_s. That's not even considering, of course, the weight of the rocket structure itself, the extra work required to overcome gravity, and atmospheric air drag, which increases the ratio of total mass to payload.

b) Conversely, If it is desired to estimate the final velocity v_s of a body of mass m_s = 1500 kg transporting a known amount of propellant m_p = 25000 kg expelled at a velocity v_p = 3.8 km/s, then Eq. (32) is applied to solve the problem as sown bellow:

$$v_s = v_p \cdot \ln\left(1 + \frac{m_p}{m_s}\right) = 3.8(km/s) \cdot \ln\left(1 + \frac{25000\ (kg)}{1500\ (kg)}\right) \quad = 10.9\ (km/s) \tag{37}$$

Therefore, the final speed reached is 10.9 km/s.

3.4.2 Modelling the transient dynamics state of a spacecraft

Conventionally the spaceship structures) exhibit two main masses: a constant mass or "dry mass" (include structural and payload) and a variable mass "wet mass" due to (propellant fluid which is liquefied before expanding). While in general the fixed mass is due to the spacecraft payload and its own structure and equipment, a highly variable mass that is equivalent to at least ten times the fixed masses is due to propellant fluid. The modelling process considers the propellant mass variation as a time-varying parameter. The rate of variation is such that the mass due to the propellant fluid is several times higher than the mass due to the structure and its payload. To describe the dynamics of a spacecraft we accept a notation related to the nature of the parameters to be used in the modelling tasks, according to the Table 15.

The amount of propellant fluid is stored into special reservoirs.). Thus, the total mass of the spacecraft which includes structural and propellant fluid masses which include dry and wet masses is

$$m_{T(t)} = m_s + m_p = m_s + m_{p\_init} - \dot{m}_p \cdot t \tag{38}$$

Where wet or propellant mass modelled as a time-varying model $m_{p(t)}$ is

$$m_{p_{(t)}} = m_{p\_init} - \dot{m}_p \cdot t$$

In order to simulate the actual conditions, it is possible to obtain the dynamic model capable to describe the spacecraft dynamics under absence of gravity effects (e.g. acceleration, velocity and space). The force balance involved in the thrust model yields

$$F = m_T \frac{dv_s}{dt} + \beta_{(h)} V_s \tag{39}$$

Outside of Earth's airspace, where the gravitational effect at the level of interplanetary transport dynamics and the terrestrial effects of the atmosphere associated with air friction due to drag are negligible, the thrust force can be restricted to a simple model such as:

$$F = m_T \frac{dv_s}{dt} \tag{40}$$

From the thrust estimation by Eq. (25) follows that a thermo-mechanic description yields

$$F = \dot{m}_p \cdot \sqrt{V_i^2 + 2 \cdot (h_i - h_e)} \tag{41}$$

Therefore the spacecraft velocity can be estimated by equaling both thrust forces Eq. (24) and (26), yielding

$$m_T \frac{dv_s}{dt} + \beta_{(h)} V_s = \dot{m}_p \cdot \sqrt{V_i^2 + 2 \cdot (h_i - h_e)} \tag{42}$$

Consequently from Eq. (42) the actual spacecraft velocity is obtained from its dynamic model as a recurrent dynamic function

$$\frac{dv_s}{dt} = \frac{1}{m_T}\left(\dot{m}_p \cdot \sqrt{V_i^2 + 2 \cdot (h_i - h_e)} - \beta_{(h)} V_s \right) \tag{43}$$

or optionally taking into account that the actual amount of propellant is time-variant, according to Eq. (38) follows that

$$\frac{dv_s}{dt} = \frac{1}{m_s + m_{p\_init} - \cdot \dot{m}_p \cdot t}\left(\dot{m}_p \cdot \sqrt{V_i^2 + 2 \cdot (h_i - h_e)} - \beta_{(h)} V_s \right) \tag{44}$$

Optionally we have also,

$$\frac{dv_s}{dt} = \frac{1}{m_s + m_{p\_init} - \cdot \dot{m}_p \cdot t}\left(\dot{m}_p \cdot v_e + (p_e - p_o) \cdot A_e - \beta_{(h)} v_s \right) \tag{45}$$

which, simplifying by neglecting certain parameters or considering the restriction given by Eq. (43), such as drag and the effect of exhaust pressure, Eq. (44) yields

$$\frac{dv_s}{dt} \approx \frac{1}{m_s + m_{p\_init} - \cdot \dot{m}_p \cdot t}\left(\dot{m}_p \cdot v_e \right)$$, or

$$\frac{dv_s}{dt} \approx \frac{1}{m_s + m_{p\_initt} - \cdot \dot{m}_p \cdot t}\left(\dot{m}_p \cdot \sqrt{2 \cdot (h_i - h_e)} \right) \tag{46}$$

By conveniently adjusting the parameters of equations (44) and/or (45) (some of them time-variant) it is possible to estimate (predict) acceptable results such as (instantaneous acceleration, speeds and current estimated position) through computer simulation. Real-time self-adaptive models are preferred since, fortunately, spatial dynamic math-models —without disturbances— are mostly deterministic. In any case, based on the existing dynamic model, the availability of parity equations facilitates the diagnosis of the vehicle's dynamic state, which makes it easier to make decisions and correct or adapt relevant or crucial parameters of the propulsion system.

3.5 Case studies regarding to propulsion techniques

The results presented in this study are based on the assumption of ideal propellant behavior. This means that there is a significant difference between the ideal results and those that might be observed in reality. This difference necessitates correcting propulsive models by considering propulsive efficiency, which has not been taken into account in this case.

3.5.1 Thrust and power estimation for H2 as propellant fluid

Recall that in the previous section, the thrust (F) in metric tons (t) produced by a propellant fluid as a function of the propellant velocity (m/s) and the mass flow rate ($\dot{m}_p$) in kg/s is expressed as: F= Thrust = $\dot{m}_p$ v_p . The power (P) in megawatts (MW) produced by a propellant fluid as a function of the enthalpy change (kJ/kg) and the mass flow rate ($\dot{m}_p$) in kg/s is expressed as: P = Power = $\dot{m}_p$ .w = $\dot{m}_p$ Δh

The specific heat capacity of propellant fluids including H_2 and N_2 varies considerably with large temperature changes. Therefore, it is not a linear function. Table 16 highlights the nonlinearity of the specific heat at constant pressure as the temperature increases for hydrogen as propellant fluid. Consequently, the enthalpy change at high temperatures is a nonlinear function that must be considered when estimating thrust and power requirements.

Table 16: The propellant ideal speed reached in a nozzle as function of the enthalpy drop due to an adiabatic-isentropic expansion considering H_2 as real gas.

T_{in}(K)	Cp (kJ/kg. K)	h_{in}(kJ/kg)	T_{out}(K)	Cp (kJ/kg. K)	h_{out}(kJ/kg)	Δh(kJ/kg)	Vp(m/s)
500	13.97	6983.7	170	13.2	2243.03	4740.7	3079.2
1000	15.06	15064.8	170	13.2	2243.03	12821.8	5064.0
1500	16.07	24109.9	170	13.2	2243.03	21866.9	6613.1
2000	16.99	33985.3	170	13.2	2243.03	31742.3	7967.7
2500	17.82	44557.6	170	13.2	2243.03	42314.5	9199.4
3000	18.56	55693.1	170	13.2	2243.03	53450.1	10339.3
4000	19.78	79119.8	170	13.2	2243.03	76876.7	12399.7
6000	21.14	126856.4	170	13.2	2243.03	124613.4	15786.9

As mentioned earlier, over significant operating temperature ranges for real gases, specific heat capacity is a nonlinear function of temperature. The nonlinearity of specific heat at constant pressure as a function of temperature is shown in the last column of Table 16, as well as in Fig. 9. The effect of the nonlinearity of the actual specific heat (Cp) affects the propellant fluid velocity and consequently the specific impulse, which is relevant for correlating thrust forces. As shown in Table 16, the enthalpy drop is function of the temperature drop.

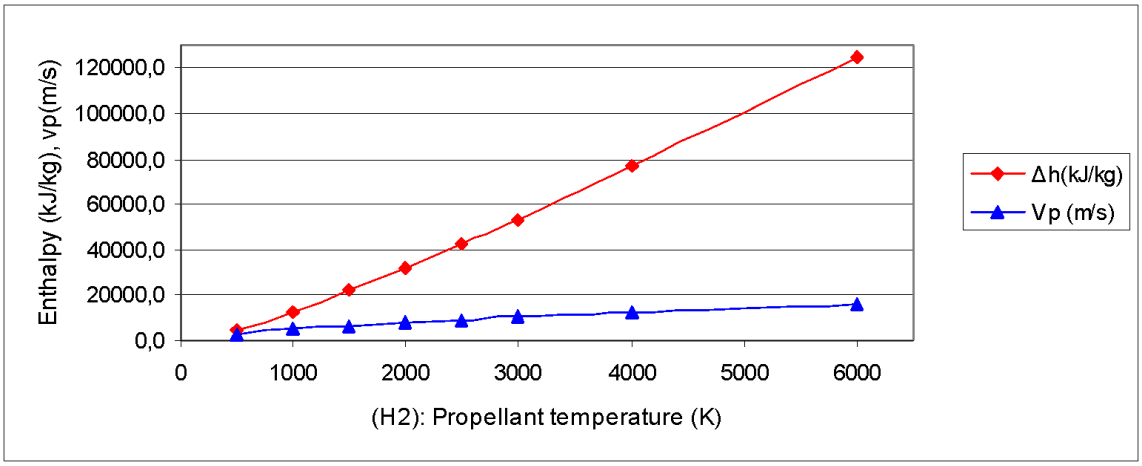

Figure 9: Illustration of the real evolution of the enthalpy as function of temperature based on data depicted in Table 16 for H_2 as propellant fluid

Table 17: illustration of the thrust in metric tons (t) as function of propellant temperature (K) and mass flow rate ($\dot{m}_p$) expressed in kg/s for H_2 as real propellant fluid.

Tin(K)	$\dot{m}_p$: 10 kg/s	$\dot{m}_p$: 25 kg/s;	$\dot{m}_p$: 50 kg/s	$\dot{m}_p$: 100 kg/s	$\dot{m}_p$: 200 kg/s
500	3.08	7.70	15.40	30.79	61.58
1000	5.06	12.66	25.32	50.64	101.28
1500	6.61	16.53	33.07	66.13	132.26
2000	7.97	19.92	39.84	79.68	159.35
2500	9.20	23.00	46.00	91.99	183.99
3000	10.34	25.85	51.70	103.39	206.79

4000	12.40	31.00	62.00	124.00	247.99
6000	15.79	39.47	78.93	157.87	315.74

Fig. 10 represents the thrust (F) in tons (t) as a function of the propellant temperature (K) and the mass flow rate ($\dot{m}_p$) expressed in kg/s for H_2

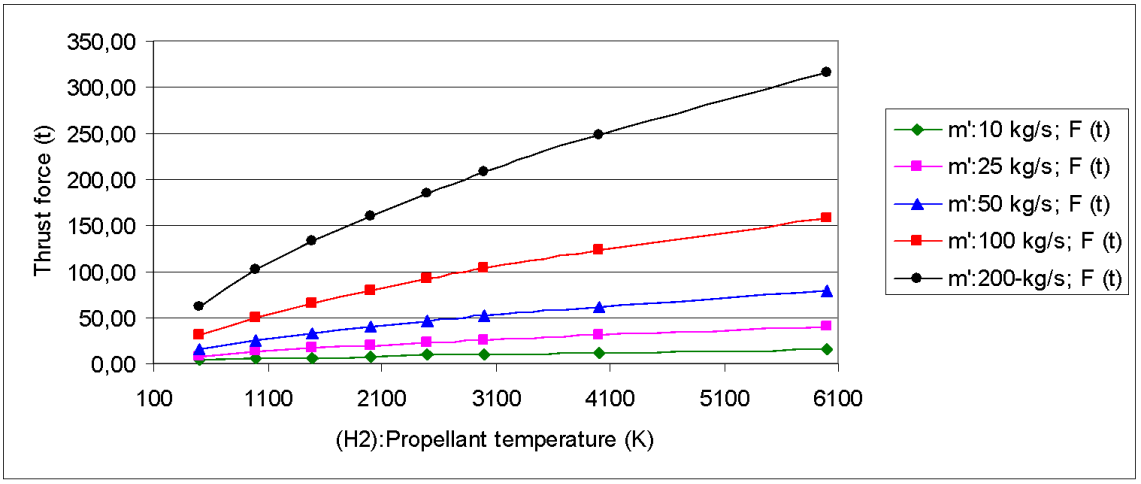

Figure 10: Illustration of the thrust (F) in tons (t) as a function of the propellant temperature and the mass flow rate ($\dot{m}_p$) expressed in kg/s for H_2 as propellant fluid

Table 18: illustration of the power (P) in (MW) as function of propellant temperature (K) and mass flow rate ($\dot{m}_p$) for H_2 as propellant fluid

Tin(K)	$\dot{m}_p$ r:10 kg/s	$\dot{m}_p$:25 kg/s	$\dot{m}_p$:50 kg/s	$\dot{m}_p$:100 kg/s	$\dot{m}_p$:200 kg/s
500	47.41	118.52	237.03	474.07	948.13
1000	128.22	320.55	641.09	1282.18	2564.36
1500	218.67	546.67	1093.34	2186.69	4373.37
2000	317.42	793.56	1587.11	3174.23	6348.46
2500	423.15	1057.86	2115.73	4231.45	8462.91
3000	534.50	1336.25	2672.50	5345.01	10690.01
4000	768.77	1921.92	3843.84	7687.67	15375.35
6000	1246.13	3115.34	6230.67	12461.34	24922.68

Fig. 11: illustrates the ideal power (MW) supplied as a function of the propellant's (H_2) temperature (K) and mass flow rate ($\dot{m}_p$) in kg/s. It can be observed that the magnitude of the power associated with a relatively low thrust requirement is enormous. This implies high flow rates of propellant fluid, which makes thrust tasks complex and costly, since the propellant fluid is not recoverable.

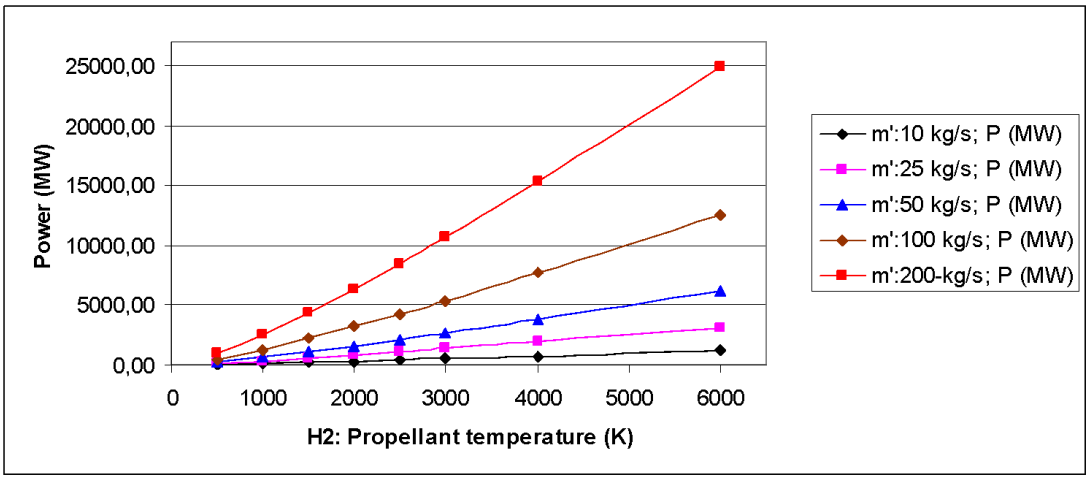

Figure 11: Illustration of the power (P) in MW as a function of the propellant temperature and the mass flow rate ($\dot{m}_p$) expressed in kg/s for hydrogen

3.5.2 Thrust and power estimation for N_2 as propellant fluid

Table 19: The propellant ideal speed reached in a nozzle as function of the enthalpy drop due to an adiabatic-isentropic expansion considering N_2 as real gas. The enthalpy drop is function of the temperature drop

Tp(K)	Cp(kJ/kg-K)	hi(kJ/kg)	Te(K)	Cp(kJ/kg-K)	hi(kJ/kg)	Δh(kJ/kg)	Vp (m/s)
500	1.056	528.0	200	1.039	207.80	320.2	800.2
1000	1.167	1167.0	200	1.039	207.80	959.2	1385.1
1500	1.244	1866.0	200	1.039	207.80	1658.2	1821.1
2000	1.284	2568.0	200	1.039	207.80	2360.2	2172.6
2500	1.307	3267.5	200	1.039	207.80	3059.7	2473.7
3000	1.323	3969.0	200	1.039	207.80	3761.2	2742.7
4000	1.342	5368.0	200	1.039	207.80	5160.2	3212.5
6000	1.369	8214.0	200	1.039	207.80	8006.2	4001.5

As shown in Table 19, the enthalpy drops responsible for the propellant fluid velocity and consequently responsible for the thrust is a function of the temperature drop across the nozzle.

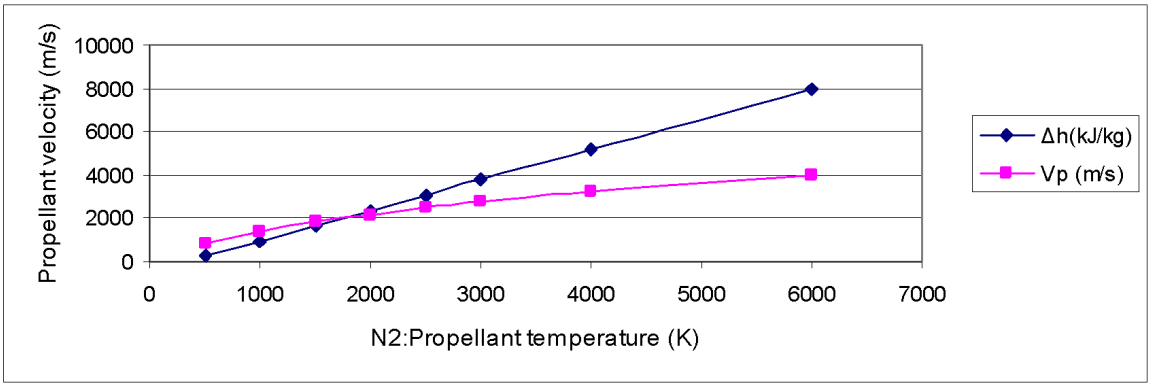

Figure 12: Illustration of the real evolution of the enthalpy as function of temperature based on data depicted in Table 19 for H_2 as propellant fluid

Table 20: illustration of the thrust in metric tons (t) as function of propellant fluid temperature (K) and mass flow rate ($\dot{m}_p$) expressed in kg/s for N_2 as real propellant fluid.

Ti(K)	$\dot{m}_p$: 10 kg/s	$\dot{m}_p$: 25 kg/s	$\dot{m}_p$: 50 kg/s	$\dot{m}_p$: 100 kg/s	$\dot{m}_p$: 200-kg/s
500	0.80	2.00	4.00	8.00	16.00
1000	1.39	3.46	6.93	13.85	27.70
1500	1.82	4.55	9.11	18.21	36.42
2000	2.17	5.43	10.86	21.73	43.45
2500	2.47	6.18	12.37	24.74	49.47
3000	2.74	6.86	13.71	27.43	54.85
4000	3.21	8.03	16.06	32.13	64.25
6000	4.00	10.00	20.01	40.02	80.03

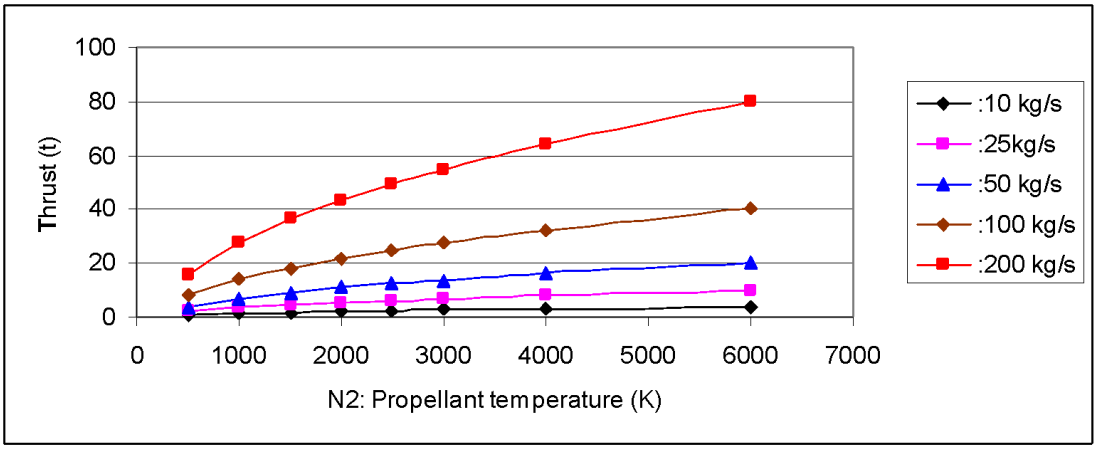

Figure 13: Illustration of the thrust (F) in tons (t) as a function of the propellant temperature (K) and the mass flow rate ($\dot{m}_p$) expressed in kg/s for hydrogen for N_2 as propellant fluid

Table 21 and Figure 14 show the power required as a function of the propellant mass flow rate and the exhaust temperature through the propulsion nozzle. It is considered that, in practice, a temperature of 3000 K can be sustained for an extended period to achieve a high steady-state transit speed.

Table 21: illustration of the power (P) in (MW) as function of propellant temperature (K) and mass flow rate ($\dot{m}_p$) for N_2 as real propellant fluid

Ti(K)	$\dot{m}_p$:10 kg/s	$\dot{m}_p$:25 kg/s	$\dot{m}_p$:50 kg/s	$\dot{m}_p$:100 kg/s	$\dot{m}_p$:200 kg/s
500	3.20	8.01	16.01	32.02	64.04
1000	9.59	23.98	47.96	95.92	191.84
1500	16.58	41.46	82.91	165.82	331.64
2000	23.60	59.01	118.01	236.02	472.04
2500	30.60	76.49	152.99	305.97	611.94
3000	37.61	94.03	188.06	376.12	752.24

4000	51.60	129.01	258.01	516.02	1032.04
6000	80.06	200.16	400.31	800.62	1601.24

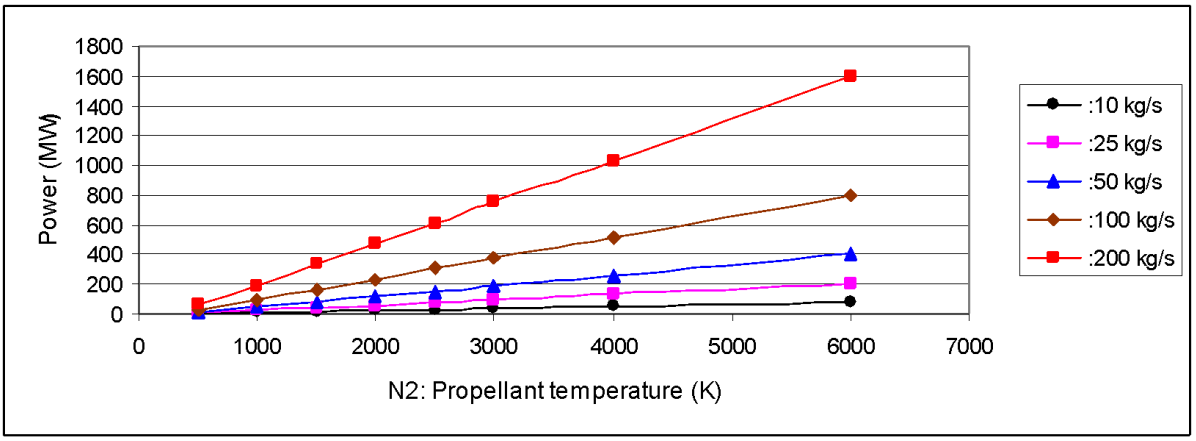

Figure 14: Illustration of the power (P) in MW as a function of the propellant temperature and the mass flow rate ($\dot{m}_p$) expressed in kg/s for H_2 as propellant fluid

Both Table 21 and Figure 14 show that the power required to provide a certain thrust force using nitrogen as the propellant fluid is surprisingly high. Essentially, the ultimate goal of the propulsion problem is to achieve the required speed with the minimum propellant weight.

3.6 Comparative data between temperatures and propellant fluids

Specific impulse (I_{sp}) is a propulsion performance parameter. It is proportional to the exhaust velocity of the propellant fluid. Therefore, the propellant's exhaust velocity is also a good parameter for evaluating its performance. Therefore, Table 22 and Fig.15 show a comparison between hydrogen and nitrogen as propellant fluids. The significant difference between the two fluids is highlighted.

5.6.1 Specific Impulse (Isp) as a reference or index of merit or efficiency.

Table 22: Specific impulse for H_2 and N_2 as propellant fluids

T(K)	H_2:Isp (s)	N_2:Isp (s)
500	313.9	81.6
1000	516.2	141.2
1500	674.1	185.6
2000	812.2	221.5
2500	937.8	252.2
3000	1053.9	279.6
4000	1264.0	327.5
6000	1609.3	408.0

Specific impulse can be considered a propulsion benchmark, as it is proportional to the propellant velocity. This means that a high propellant velocity, obtained through an adiabatic expansion process via a nozzle, equates to a high specific impulse. A higher specific impulse means the engine is more efficient, producing more thrust for the same amount of propellant.

For conventional rocket engines ranges from approximately 200 to over 3.000 seconds, depending on the technology, with chemical rockets typically operating between 200–450 seconds and advanced electric

propulsion reaching thousands of seconds. It measures efficiency as the thrust generated per unit of propellant consumed.

A previously commented, the corresponding expulsion velocities v_p of the respective propellant fluids depicted in Table 22 and Fig.15 are directly proportional to the specific impulses I_{sp}; e.g., v_p=g. I_{sp}.

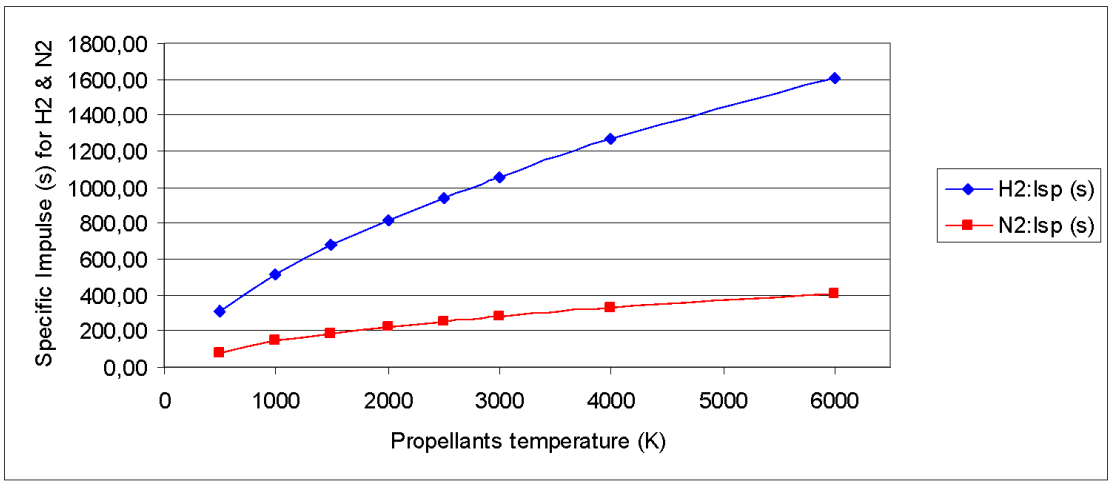

Figure 15: Illustration of the evolution of the specific impulse of H_2 and N_2 as propellant fluids as a function of temperature.

3.6.2 Achievable ISP ranges by propulsion technology

Solid-Propellant Rockets: 200–300 s (e.g., boosters, upper stages).

Liquid-Propellant Rockets: 300–450 s.

Hydrolox ~450 s (highest for chemical).

Metholox ~320 s.

Kerolox ~295 s.

Hybrid Rockets: Typically higher than solid rockets.

SSPM-based Rockets: Potential for ~1000+ s with H_2 as propellant and Tp > 3000 K.

SSPM-based Rockets supplying power to the Electric/Ion Thrusters: 1.000–3.000+ s.

SSPM-based Rockets supplying power to advanced propulsion (e.g., VASIMR): Can exceed 10.000–30.000 s.

3.6.3 Critical analysis of results concerning VASIMR-based technologies

The Variable Specific Impulse Magneto-plasma Rocket (VASIMR) [32] is an advanced, electrodeless plasma propulsion system designed for high-power, long-duration space missions, such as human exploration of Mars. Unlike conventional chemical rockets, VASIMR uses radio waves (RF) to ionize and heat propellant (argon, xenon, or hydrogen) to extreme temperatures, creating a plasma that is accelerated by magnetic fields to generate thrust.

Core Components and Advanced Features

Three-Stage Process: The system consists of a helical plasma source (ionization), an Ion Cyclotron Resonance Heating (ICRH) booster (heating), and a magnetic nozzle (acceleration).

Variable Specific Impulse: The engine allows for in-flight optimization of exhaust velocity (specific impulse) and thrust, acting like a gearbox to balance speed and fuel efficiency.

High Power Operation: The Ad Astra Rocket Company's VX-200 prototype has demonstrated high-power operations (200 kW), achieving plasma temperatures exceeding 1 million Kelvin.

Superconducting Magnets: Advanced, high-temperature superconducting magnets are used to confine the high-energy plasma, preventing it from damaging the engine structure.

Key Advantages for Space Exploration

High-Speed Transit: Potential to reduce travel time to Mars to approximately 40–45 days.

High Fuel Efficiency: Plasma rockets, such as the VX-200, achieve high efficiency (over 60% at or above 3,000 s specific impulse).

Improved Durability: Because it is electrodeless, it avoids the erosion issues found in traditional ion thrusters.

Scalability: The technology is scalable from lower power levels (for satellite station-keeping) to multi-megawatt systems for interplanetary missions.

Current Status and Future Outlook

Development & Testing: The VX-200SS has completed long-duration, high-power firings, with a goal of achieving 100 kW continuous operation.

Application: Future applications include cargo transport, asteroid deflection, and human missions to Mars.

Power Source: While currently powered by simulated sources, full-scale deployment requires a space-worthy nuclear reactor to provide the necessary high power.

3.7 Case studies related to Tsiolkovsky's equation

The Tsiolkovsky equation is useful for analyzing the transient dynamic state of any space vehicle propelled by rockets that operate by reaction of the jet of a propellant fluid being expanded through a nozzle. According to the Tsiolkovsky equation, the steady-state transit velocity reached, v_s, is given by $\frac{v_s}{v_p} = \ln[1 + \frac{m_p}{m_s}]$, which yields a final velocity of the rocket of $v_s = v_p \cdot \ln[1 + \frac{m_p}{m_s}]$ Under mentioned initial conditions, the propellant fluid is heated and expelled at a velocity v_p, for which the rocket's transit velocity is obtained in (km/s). According to the Table 23 data, The achieved rocket speed of presented under km/s, km/h and km/d. According to the data in Table 23, it is evident that the propellant fluid expulsion speed v_p is essential to achieving a high rocket speed v_s, since there is a dependence of the rocket speed directly related to the propellant fluid expulsion speed. In this study it is used a mass of propellant (m_p) for various propellant expulsion velocities v_p. That is, an initial amount of propellant fluid, mp = 50 t, is assumed to push a spacecraft of mass ms = 10 t.

Table 23: Illustration of the final velocity (v_s) of a spacecraft (expressed in km/s, km/h and km/d) of a rocket of weight m_s=10 (t) achieved by expelling an amount of propellant fluid of 50 (t) for several propellant fluid velocities between 4-14 km/s

v_p(km/s)	I_{sp} (s)	v_s(km/s)	v_s(km/h)	v_s(km/d)
4	407.7	7,17	25.801	619.232
6	611.6	10,75	38.702	928.848
8	815,5	14,33	51.603	1.238.464
10	1019.4	17,92	64.503	1.548.080
12	1223.2	21,50	77.404	1.857.696
14	1427.1	25,08	90.305	2.167.312

Therefore, the importance of the study lies in the need to achieve a high gas expulsion speed with the minimum amount of propellant fluid.

With regard to the case study of Table 23, let's consider a quantity of propellant fluid, expressed in tons (t); for example, 50 t. This is intended to propel a rocket or spacecraft in transit without gravitational interactions or losses, whose structural weight (constant) is 10 t. According to the Tsiolkovsky equation, the steady-state transit velocity reached, v_s, is shown in the Fig.16. Under mentioned initial conditions, the propellant fluid is heated and expelled at a velocity v_p, for which the rocket's transit velocity is obtained in (km/s).

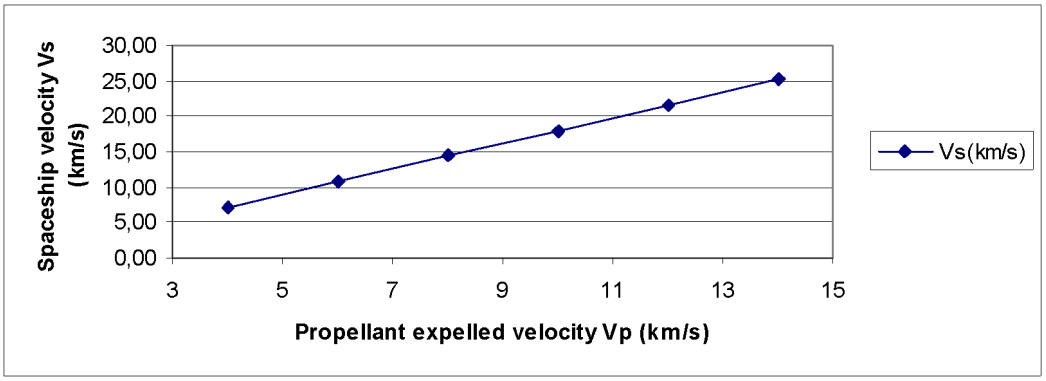

Figure 16: Illustration of the final velocity (v_s) of the rocket, whose mass (m_s) is determined for each quantity of propellant (m_p) consumed at the ejection velocity (v_p.)

3.7.1 Analysis of the transient and steady-states transit velocity of a rocket assisted spacecraft

The simple procedure shown in Table 23 and Figure 16, respectively, allows us to estimate the propellant and spacecraft masses required reaching a transit velocity and, consequently, to estimate the time needed to reach the destination within a known time.

Table 24 shows the steady-state transit velocities achievable with H2 and N2 as propellant fluids heated to 3000 K as a function of the propellant quantities used. It can be seen that the amount of hydrogen required to reach a certain speed is much lower than that required for nitrogen.

Table 24: Steady-state transit velocities (in km per second, hour and day) achievable with **H_2** and **N_2** as propellant fluids heated to 3000 K

H_2: m_p (t)	m_s (t)	V_p(km/s)	ratio(m_p/m_s)	v_s(km/s)	v_s(km/h)	v_s(km/d)
10	10	10.34	1	7.2	25.802	619.241
20	10	10.34	2	11.4	40.895	981.474
40	10	10.34	4	16.6	59.910	1.437.833
80	10	10.34	8	22.7	81.789	1.962.948
120	10	10.34	12	26.5	95.478	2.291.464
160	10	10.34	16	29.3	105.464	2.531.125
N_2: m_p (t)	m_s (t)	v_p(km/s)	ratio(m_p/m_s)	v_s(km/s)	v_s(km/h)	v_s(km/d)
10	10	2.74	1	1.9	6.837	164.093
20	10	2.74	2	3.0	10.837	260.081
40	10	2.74	4	4.4	15.875	381.012
80	10	2.74	8	6.0	21.673	520.162
120	10	2.74	12	7.0	25.301	607.216
160	10	2.74	16	7.8	27.947	670.724

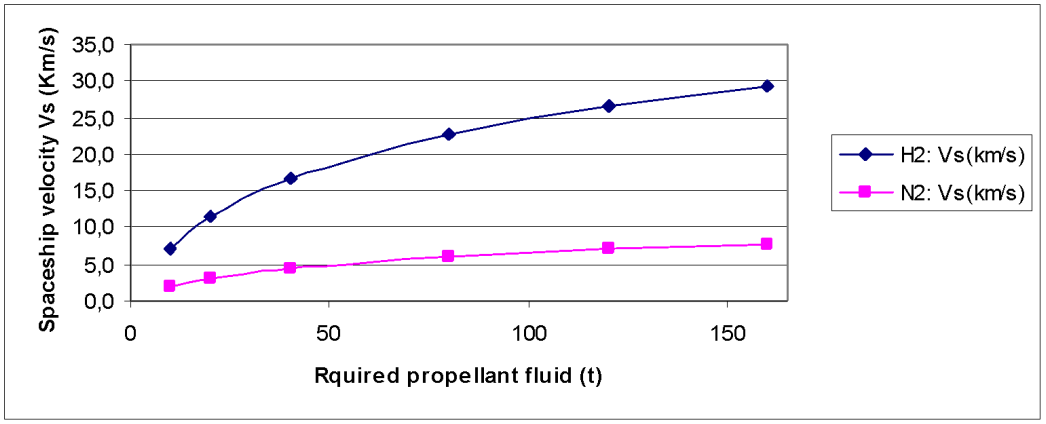

Figure 17: Illustration of the final velocity

3.7.2 Analysis of the rocket transient dynamics

According to the Tsiolkovsky equation, the transient dynamics state of a space ship or rocket can be analysed by means of the Tsiolkovsky relation between propellant mass m_p and rocket structure mass m_s according to the expression: $\frac{m_p}{m_s} = (e^{(v_s / v_p)} - 1)$. Under mentioned initial conditions (v_s and v_p), the propellant fluid is heated and expelled at a velocity v_p, for which the rocket's transit velocity is obtained in (km/s).

Table 25: illustration of the required amount of propellant fluid mass m_p as function of the rocket increment of speed achieved, for several rocket structure masses, respectively 40, 20, 10 and 5(t)

Δv_s (km/s)	m_s=40(t)	m_s=20(t)	m_s=10(t)	m_s=5(t)
10.2	84.24	42.12	21.06	10.53
9.2	71.17	35.59	17.79	8.90
7.2	49.02	24.51	12.26	6.13
5.2	31.28	15.64	7.82	3.91
3.2	17.08	8.54	4.27	2.13
1.2	5.71	2.85	1.43	0.71

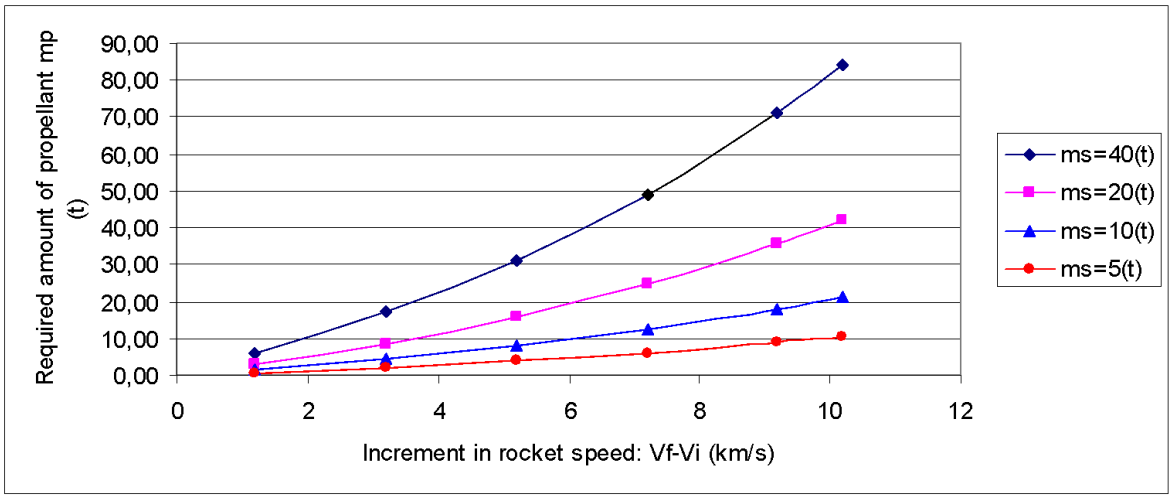

Figure 18: Illustrates the data shown in Table 25, that is the required amount of propellant fluid mass m_p as function of the rocket increment of speed achieved, for several rocket structure masses, respectively 40, 20, 10 and 5(t) respectively

According to the data in Table 25 and represented graphically in Fig. 18, the amount of propellant needed to increase the rocket's speed to the desired speed (e.g., observing Fig. 18, the rocket's speed increases to the Earth escape velocity of 11.2 km/s, from an initial speed of vi) is also shown.

3.8 Concept of a technically viable self-sufficient jet propulsion system

The aim of this study was a preliminary study for replacing nuclear energy with self-sustaining energy sources. This involves the elimination of both nuclear thermal power (NTP) and nuclear electrical power (NEP). Therefore, this section briefly describes a schematic of the proposed self-propelled jet system preliminary prototype, which consists of two main components arranged as shown in Figure 19:

-- Self-sufficient electric power generator system (SSPG) illustrated in Fig. 5, which is based on cascaded Pulse Gas Turbines (PGT) and

-- Jet propulsion system (JPS) driven by a SSPG.

The SSPG is responsible for supplying electrical power to both the propulsion systems and onboard power services.

The JPS consists of a conventional nozzle-based thruster that operates primarily with heated hydrogen as the propellant. It is responsible for the rocket's thrust. Propellant fluid is heated with electric power from a SSPG.

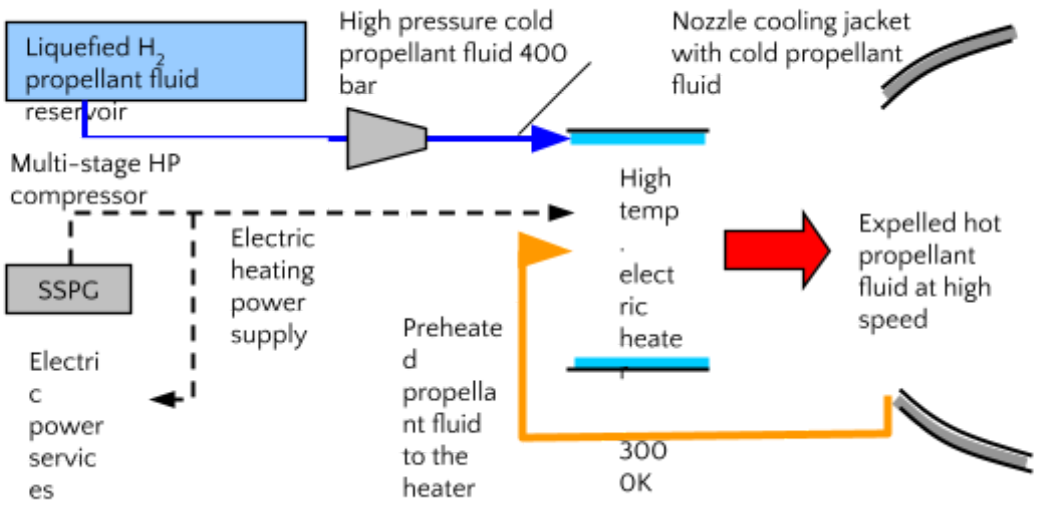

Figure 19: A simplified diagram illustrating the JPS assisted by an SSPG

4. Analysis of results

The article proposes a preliminary design task that aims for a disruptive change in both: the supply of self-sustaining energy and an electricity-based propulsion technology that allows replacing nuclear-based systems with SSPM technologies.

4.1 Space-Based Power System based on cascaded Pulsed Gas Turbine (PGT)

The modelling task of a Space-Based Power System with Cascaded Pulse-Based Gas Turbines has been described in section 2. Therefore, it has been shown, that section 2 is focused on power generation systems for space applications that can replace current nuclear power generation systems. It presents a novel power generation technology called the Pulsed Gas Turbine **(PGT)** and its integration into a larger system called a Self-Sustaining Power Machine **(SSPM)**.

Key Concepts and In-Depth Analysis: Throughout section 2, we have evolved from moving from theoretical concept to detailed analysis and finally to practical application (scaling for space missions). Its primary purpose is to introduce, model, and analyse the performance of a cascaded PGT system. The core argument is that by using a unique thermodynamic cycle (sVsVs) and cascading multiple Power Units (PUs), the system can achieve high thermal efficiency and self-sustainability, making it ideal for high-demand applications like space propulsion and resource exploitation, where it could potentially replace nuclear power sources.

The Key Concepts and In-Depth Analysis include:

4.1.1 The Pulsed Gas Turbine (PGT) and the sVsVs Cycle

Core Innovation: The PGT moves away from traditional constant-pressure combustion turbines. It operates intermittently using "barothermal pulses"—positive pressure pulses from isochoric (constant volume) heating and negative pressure pulses from isochoric cooling.

The sVsVs Cycle: This is the thermodynamic cycle at the heart of each Power Unit (PU).

Acronym: "s" stands for isentropic (constant entropy), and "V" stands for isochoric (constant volume).

Sequence:

The cycle is a hybrid of open (mass transfer) and closed processes:

1-2 (s): Isentropic compression (pumping TWF to a hot reservoir).

2-3 (V): Isochoric heat addition (heating TWF in a reservoir).

3-4 (s): Isentropic expansion (TWF expands through turbine, producing work).

4-5 (V): Isochoric heat extraction (cooling TWF in a reservoir).

5-1 (s): Isentropic contraction (cooled TWF contracts, producing more work).

Advantages: The text highlights key benefits: no phase change in the working fluid, simplified design, reduced need for blade cooling, and, most importantly, Useful work by vacuum-induced thermal contraction of thermal working fluid, and consequently, a thermal efficiency not constrained by the Carnot efficiency in the same way as conventional cycles. In fact, it claims efficiency is higher for smaller temperature ranges.

4.1.2 The Cascaded Architecture (SSPM)

Concept: The concept is based on the idea that, to maximize efficiency and utilize waste heat, multiple PGT-based power units (PUs) are coupled on a single shaft in a cascade. This is the Self-Sustaining Power Machine (SSPM).

Operation: The system operates by recovering the heat rejected during the cooling process of one wastewater treatment unit and using it as input heat for the next unit downstream. This creates a highly efficient waste heat recovery system, making the plant's operation self-sustaining.

Constant Temperature Drop (T_D): A key design parameter is the constant temperature drop $\mathbf{T_D}$ between the inlet and outlet of each cascaded PU. This ensures all PUs has a similar structure and that the rotating machinery (turbines) can be identical, reducing manufacturing costs.

4.1.3 Detailed Parametric Analysis and Case Studies

This is the core of the analysis, comparing four different SSPM configurations based on the constant temperature drop ($\mathbf{T_D}$) per PU.

Methodology: Four case studies are run with a top temperature of 1000 K, a bottom temperature of 350 K, and varying $\mathbf{T_D}$ values: 50 K, 75 K, 100 K, and 150 K. The working fluid is helium.

Key Findings from Tables 3-11:

Number of PUs: The number of PUs in the cascade is inversely proportional to $\mathbf{T_D}$ (NPU = (1000-350)/ $\mathbf{T_D}$). A smaller $\mathbf{T_D}$ means more PUs (e.g., 13 PUs for a 50 K drop).

Total Useful Work: The total mechanical work produced by the cascade peaks at a $\mathbf{T_D}$ of 100 K (Case 3 with 7 PUs), as shown by the black curve in Figure 6.

Net Useful Work: However, a portion of this work must be fed back ("Feedback Heat") to power the system's internal pumps and compressors. The net useful work (profit) peaks at a $\mathbf{T_D}$ of 75 K (Case 2 with 9 PUs), as shown by the red curve in Figure 6.

Optimization Problem: This creates a design trade-off. Case 2 (9 PUs) gives the highest net power output, but Case 3 (7 PUs) gives a very similar net output with two fewer PUs. Fewer PUs means lower manufacturing and maintenance costs, making Case 3 potentially more attractive from an engineering economics perspective, despite its slightly lower net output.

4.1.4 Application: Scaling for Space Propulsion

Objective: The final section bridges the gap between theoretical analysis and a real-world mission. It outlines how to scale the chosen SSPM design (Case 2 or 3) to meet the power demands of a spacecraft.

Scaling Process:

1 Identify Demand: Determine the required power (MW) for services like transport and resource exploitation.

2 Use Specific Work: The analysis provides the specific work (kJ/kg) for the SSPM. Power is calculated as: Power = Mass Flow Rate (kg/s)*Specific Work (kJ/kg which yields (kJ/s) = kW.

3 Scale Volume: The thermodynamic volume of the system (V_{SSPM} in m^3/kg) is a key metric. To increase the mass flow rate (and thus power), the physical size of the reservoirs and TWF volume must be scaled proportionally. Tables 14 and 15 show how power scales with mass flow rate and cycle time for the two candidate cases.

To conclude, this scaling methodology allows engineers to estimate the size and mass of the SSPM required generating, for example, 150 MW, which is presented as a viable alternative to nuclear power for ambitious space exploration.

4.2 Analysis of Results concerning section Spacecraft Propulsion System Modelling

The modelling task of a Spacecraft Propulsion System characterized by using jet propulsion without propellant combustion has been described in section 3.

It has been shown that section 3 provides a comprehensive, though ideal, analysis of a spacecraft propulsion system. It establishes the known fundamental physical principles, derives known key mathematical relationships, and then applies them to case studies to quantify performance parameters for different propellants and mission scenarios. The core objective is to determine the electrical power demand required to generate sufficient thrust for space travel while managing the critical constraint of non-recoverable propellant mass. Therefore, the analysis is structured in a logical flow from fundamental theory to practical application and comparative evaluation.

4.2.1 Fundamental Relationships and the Core Trade-off

The analysis begins by grounding the propulsion model in Newton's laws, leading to two pivotal equations:

Thrust Equation (Ideal Vacuum): $F = \dot{m} \cdot v_e$

This establishes a direct, linear relationship between thrust (F), the mass flow rate of the propellant ($\dot{m}$), and its exhaust velocity (v_e).

Kinetic Power Equation (Ideal): $PK = (1/2) \cdot \dot{m} \cdot v_e^2$

This defines the power contained in the exhaust jet, which is proportional to the mass flow rate and the *square* of the exhaust velocity.

The text then masterfully combines these to reveal a critical inverse relationship for a constant thrust requirement (F): $P_K = (F^2) / (2 \cdot \dot{m})$

Insight: This is the central trade-off of the analysis. For a desired thrust force (F):

Using a high mass flow rate ($\dot{m}$) requires less power but consumes propellant very quickly.

Using a low mass flow rate ($\dot{m}$) is propellant-efficient but requires significantly more power to achieve the same thrust.

This trade-off frames the entire propulsion design problem as a balance between power availability (an engineering constraint) and propellant mass (a mission logistics constraint).

4.2.2 Propellant Performance and the Role of Thermodynamics

To move beyond simple relationships, the model incorporates thermodynamics, treating the nozzle expansion as an isentropic process. The key finding is that exhaust velocity (v_e). It is derived from the enthalpy drop (Δh) across the nozzle of the preheated propellant fluid: $v_e \cdot \sqrt{2 \cdot \Delta h}$

This thermodynamic link is crucial because Δh is a function of the propellant's specific heat (Cp) and the temperature drop across the nozzle. The text correctly notes that Cp is not constant but a nonlinear function of temperature for real gases, a factor that becomes highly significant at the extreme temperatures required for high-performance propulsion.

4.2.3 Comparative Analysis of Propellants: H_2 vs. N_2 (Sections 3.5, 3.6)

The theoretical framework is applied to two distinct propellants, hydrogen (H_2) and nitrogen (N_2), heated to various temperatures. The results, presented in Tables 16-22 and Figures 9-15, are striking and form the core of the study's practical conclusions.

Key Result 1: Exhaust Velocity and Specific Impulse (Isp)

Hydrogen (H_2) dramatically outperforms Nitrogen (N_2). At 3000K, H_2 achieves an exhaust velocity of 10.34 km/s (Isp ~1054 s), while N_2 only reaches 2.74 km/s (Isp ~280 s).This is because H_2's much lower molecular mass results in a higher exhaust velocity for the same enthalpy drop.

The nonlinear increase in Cp with temperature for H_2 means that incremental increases in temperature yield progressively larger gains in exhaust velocity and Isp, a key insight for high-temperature reactor design.

Key Result 2: Thrust Generation

For a given mass flow rate ($\dot{m}$), thrust is directly proportional to the exhaust velocity. Therefore, H_2 produces significantly more thrust than N_2 under the same conditions. For example, at $\dot{m}$ =100 kg/s and 3000K, H_2 generates ~103.4 tons of thrust, while N_2 generates only ~27.4 tons (Tables 17 & 20).

Key Result 3: The Staggering Power Demand (The "Dilemma")

This is the most critical operational finding. The power required to heat the propellant to these temperatures is enormous.

To generate the ~103.4 tons of thrust with H_2 ($\dot{m}$ =100 kg/s, 3000K), the required ideal power is 5345 MW (Table 18), which is equivalent to 5,345 GW.

This confirms the core trade-off: achieving high thrust with a reasonable mass flow rate (i.e., being propellant-efficient) requires a power output on a scale that is currently unimaginable for a spacecraft.

The analysis shows that using a higher mass flow rate would reduce the power requirement (as per $P = F^2/2\dot{m}$), but this would mean consuming the propellant at an impossibly fast rate.

4.2.4 Mission Analysis with the Tsiolkovsky Rocket Equation (Sections 3.4, 3.7)

The Tsiolkovsky equation, $\Delta v = ve * \ln(m_0/m_f)$, is used to translate propellant performance into mission capabilities. This analysis highlights the tyranny of the rocket equation.

Key Result 4: The Exponential Cost of Speed

To achieve a high spacecraft velocity (Δv), the required propellant mass grows exponentially with the desired Δv.

Example 1: To reach escape velocity (~12 km/s) for a 2000 kg payload with a propellant exhaust velocity of 4 km/s, a staggering **38,117 kg of propellant** is needed —a propellant-to-payload ratio of nearly 20:1 (Section 3.4.1). This does not even include the structural mass of the rocket itself.

This exponential relationship is clearly illustrated in Table 25 and Figure 18, which show how the required propellant mass skyrockets as the desired change in velocity (Δv_s) increases, especially for heavier spacecraft structures (ms).

Key Result 5: Mission Performance with Different Propellants

Tables 23 and 24, along with Figures 16 and 17, demonstrate how the choice of propellant dictates mission feasibility. With 50 tons of propellant to push a 10-ton spacecraft, H_2 heated to 3000K can achieve a final velocity of ~26.5 km/s. N_2 under the same conditions can only reach ~7.0 km/s, a massive difference in transit time and mission reach.

5 Overall Conclusions and Implications

This article proposes a viable Self-Sustaining Power Machine (SSPM) capable of supplying electrical power to propel a rocket or spacecraft, replacing both thermal and electric nuclear propulsion systems. Both the electrical generation system and the propulsion system have been studied in sections 2 and 3, respectively, and the following conclusions are drawn from their results:

5.1 Conclusions regarding the self-generation power system described in section 3

Therefore, the results provide a comprehensive and rigorous analysis of a cutting-edge power generation concept. It successfully:

1 Introduces a novel thermodynamic cycle (sVsVs).

2 Explains its implementation in a cascaded, self-sustaining architecture (SSPM).

3 Performs a detailed parametric analysis to identify optimal operating conditions, revealing a critical trade-off between peak net power output and system complexity (number of PUs).

4 Concludes by demonstrating a practical methodology for scaling the technology to meet the immense power demands of future space missions, positioning it as a strong candidate to replace nuclear reactors.

5.2 Conclusions regarding the self-propulsion system described in section 4

5.2.1 The Propulsion Paradox is Real and Quantified**:** The analysis successfully quantifies the fundamental dilemma of space propulsion. Achieving high speed with a low propellant mass (high Isp) requires an extraordinarily high-power input. Conversely, using less power requires consuming an impractically large amount of propellant.

5.2.2 Hydrogen is the Superior Propellant: For a thermo-mechanical system, hydrogen offers vastly superior performance (Isp, exhaust velocity, thrust for a given $\dot{m}$) compared to a heavier gas like nitrogen. Its low molecular mass is the primary reason.

5.2.3 Power, Not Thrust, is the Ultimate Constraint: The analysis reveals that the primary engineering challenge is not generating thrust, but generating the immense electrical power required to do so efficiently. The power requirements identified (in the gigawatts) point to the need for an advanced, high-energy power source, such as a space-borne nuclear reactor, as explicitly mentioned in the discussion of VASIMR technology.

5.2.4 The Model's Ideal Nature is a Limitation: The analysis is based on ideal, lossless assumptions (isentropic expansion, no friction, no gravity, no drag). The text acknowledges this, stating that real-world results would differ and require correction factors like propulsive efficiency. The actual power demand would be even higher, and the achievable thrust lower, than the values presented.

In summary, the analysis provides a rigorous, quantitative foundation for understanding spacecraft propulsion. It successfully demonstrates that while the physics are well-understood, the engineering challenge lies in the immense power requirements for efficient, high-speed travel, a challenge that current technology is only beginning to address with concepts like nuclear-powered VASIMR.

References

1. Demonstration Rocket for Sgile Cislunar Operations DRACO.

https://en.wikipedia.org/wiki/Demonstration_Rocket_for_Agile_Cislunar_Operations

2. Hall Effect vs. Ion Thruster: Electric Propulsion Explained

https://www.theleeco.com/insights/hall-effect-vs-ion-thruster-electric-propulsion-explained/

3 Hall-effect thruster. https://en.wikipedia.org/wiki/Hall-effect_thruster

4 Ion thruster. https://en.wikipedia.org/wiki/Ion_thruster Offers very high specific impulse (Isp 3000-10,000+ sec) for exceptional propellant efficiency, but generally produces low thrust, leading to long, spiral-shaped acceleration profiles.

5 Fission Surface Power. Retrieved from: https://www.nasa.gov/exploration-systems-development-mission-directorate/fission-surface-power/ and, https://www.researchgate.net/publication/322589326_NASA's_Kilopower_reactor_development_and_the_path_to_higher_power_missions .

6 List of spacecraft with electric propulsion.

https://en.wikipedia.org/wiki/List_of_spacecraft_with_electric_propulsion

7 NASA's Kilopower Reactor Development and the Path to Higher Power Missions. NASA/TM—2017-219467, March 2017. Conference: 2017 IEEE Aerospace Conference.

DOI: 10.1109/AERO.2017.7943946

8 Robert Braun, Roger Myers, Shannon Bragg-Sitton, Show all 12 authors, Alan Angleman "Space Nuclear Propulsion for Human Mars Exploration", NASEM Space Nuclear Propulsion Technologies Committee Report, released 02-12-2021, https://doi.org/10.17226/25977. Retrieved from: https://www.researchgate.net/publication/349379840_Space_Nuclear_Propulsion_for_Human_Mars_Exploration_NASEM_Space_Nuclear_Propulsion_Technologies_Committee_Report_released_02-12-2021_httpsdoiorg101722625977

9 Duchek, M.E., Boylston, A., Langford, D.*et al.* .Nuclear electric propulsion for Saturn and Enceladus science missions. *J Electr Propuls* 4, 54 (2025). https://doi.org/10.1007/s44205-025-00145-x

Chapter 3: Nuclear Electric Propulsion. Space Nuclear Propulsion for Human Mars Exploration.

10 National Academies of Sciences, Engineering, and Medicine. 2021. Washington, DC: The National Academies Press. https://doi.org/10.17226/3370.

Retrieved on 24/12/25 rom:https://www.nationalacademies.org/read/25977/chapter/5.

11. Ramon Ferreiro Garcia. Study of the disruptive design of a thermal power plant implemented by several power units coupled in cascade. Energy Technol. 2023, 2300362 (1-17). Published by Wiley-VCH GmbH. DOI: https://doi.org/10.1002/ente.202300362.

12. Ramón Ferreiro Garcia. Efficient disruptive power plant-based heat engines doing work by means of strictly isothermal closed processes. Journal of Advances in Physics Vol 22 (2024), p 30.53, ISSN: 2347-3487. https://rajpub.com/index.php/jap/article/view/9587. DOI: https://doi.org/10.24297/jap.v15i0.9587.

13. Ramón Ferreiro Garcia. Design study of a disruptive self-powered power plant prototype. Journal of Advances in Physics Vol 22 (2024), p 62.92, ISSN: 2347-3487. https://rajpub.com/index.php/jap/article/view/9596. DOI: https://doi.org/10.24297/jap.v22i.9596.

14. Ramón Ferreiro Garcia. Prototyping a Disruptive Self-Sustaining Power Plant enabled to overcome Perpetual Motion Machines. Journal of Advances in Physics Vol. 22 (2024), p 141.178, ISSN: 2347-3487. https://rajpub.com/index.php/jap/article/view/963. DOI: https://doi.org/10.24297/jap.v22i.9633.

15. Ramón Ferreiro Garcia. Prototyping Self-Sustaining Power Machines with Cascaded Power Units Composed by Pulse Gas Turbines. Journal of Advances in Physics Vol. 22 (2024), p 141.178, ISSN: 2347-3487. https://rajpub.com/index.php/jap/article/view/9648. DOI: https://doi.org/10.24297/jap.v22i.9648

16. Ramón Ferreiro Garcia. Prototyping disruptive self-sufficiency power machines composed by cascaded power units based on thermo-hydraulic actuators. Journal of Advances in Physics Vol 22 (2024), p 141.178, ISSN: 2347-3487. https://rajpub.com/index.php/jap/article/view/9662. DOI: https://doi.org/10.24297/jap.v22i.9662.

17. Ramón Ferreiro Garcia. How to violate the first law of thermodynamics with an ASE of Papain and Newcomen before it was stated by Clausius. JOURNAL OF ADVANCES IN PHYSICS, 23, 9–27. (2025) https://doi.org/10.24297/jap.v23i.9706

18. Ramon Ferreiro Garcia. Power Plants and Cycles: Advances and trends. Book (2020): ISBN: 9789390431595; DOI:10.9734/bpi/mono/978-93-90431-59-5. https://www.researchgate.net/publication/347635047_Power_Plants_and_Cycles_Advances_and_Trends

19. Ramon Ferreiro Garcia. Preliminary design task for prototyping Self-Sustaining Power Machines on Mars using local resources. Journal of Advances in Physics,23, 83-115. (2025) https://doi.org/10.24297/jap.v23i.9737

20. Ramon Ferreiro Garcia. Prototyping Studies for Self-Sufficient Power Machines with local resources from the Moon. Journal of Advances in Physics, 23, 116-146 (2025) https://doi.org/10.24297/jap.v23i.9747

21. Ramon Ferreiro Garcia. Prototyping Studies for Proposal for Prototyping Disruptive Self-Sufficient Power Engines: Harnessing "Pull" Forces. Journal of Advances in Physics, 23, 263-304 (2025) https://doi.org/10.24297/jap.v23i.9792

22 E. W. Lemmon, M. L. Huber, M. O. McLinden, NIST Reference Fluid Thermodynamic And Transport Properties - REFPROP Version 8.0, User's Guide, NIST, Boulder, CO. 2007.

23. Ramon Ferreiro Garcia. Improving the design of self-sustaining power plant prototypes through profit optimization. Journal of Advances in Physics, 23, 315-335 (2025) DOI: https://doi.org/10.24297/jap.v23i.9821.

24. Patente: Máquina térmica alternativa regenerativa de doble efecto, de procesos cerrados y abiertos y su procedimiento de operación. "Regenerative double-effect heat engine, with closed and open processes and its operating procedure". Ramon Ferreiro Garcia, Jose Carbia Carril. University of A Coruna. Número de solicitud: P201700181. Accessed at: https://consultas2.oepm.es/ceo/jsp/busqueda/busqRapida.xhtml;jsessionid=qzBIO1KHmr9+xjw8ggw8YH5X.ConsultasC1.

25. Patent: Planta térmica con máquina de doble efecto, acumuladores térmicos, convección forzada y alimentación térmica reforzada con un ciclo Brayton inverso y procedimiento de operación. Thermal power plant with double-effect machine, thermal accumulators, forced convection and reinforced thermal supply with a reverse Brayton cycle and operating procedure. Jose Carbia Carril. Ramon Ferreiro Garcia, application number P201700667 and publication number 2 696 950 B2. Accessed at: https://consultas2.oepm.es/ceo/jsp/busqueda/busqRapida.xhtml;jsessionid=MDkG1OIa9BfQrxSiImwxtYlC.ConsultasC2.

26. Patent: Procedimiento de operación de una máquina alternativa de doble efecto con adición y extracción de calor y convección forzada. Operating procedure of a double-acting reciprocating machine with heat addition and extraction and forced convection and operating procedure. Ramon Ferreiro Garcia, Jose Carbia Carril, , application number P201700718 and publication number 2 704 449 B2. Accessed at: https://consultas2.oepm.es/ceo/jsp/busqueda/busqRapida.xhtml;jsessionid=-wHy58sbfVYQutIYN8s0+IKK.ConsultasC1.

27. Patent: Planta termoeléctrica multi estructural policíclica y procedimientos de operación. "Polycyclic multi-structure thermal power plant and operating procedures". Ramon Ferreiro Garcia, Application number: P202200035 and publication number 2 956 342 B2. Accessed at: https://consultas2.oepm.es/ceo/jsp/busqueda/busqRapida.xhtml;jsessionid=-wHy58sbfVYQutIYN8s0+IKK.ConsultasC1.
https://www.researchgate.net/publication/347635047_Power_Plants_and_Cycles_Advances_and_Trends

28. Patent: Sistema de transferencia de calor para calentar y enfriar módulos de potencia acoplados en cascada de plantas termoeléctricas y procedimiento de operación. "Heat transfer system for heating and cooling cascade-coupled power modules of thermoelectric plants and operating procedure". Ramon Ferreiro Garcia. Application number: P202400002. Accessed at: https://consultas2.oepm.es/ceo/jsp/busqueda/busqRapida.xhtml;jsessionid=qzBIO1KHmr9+xjw8ggw8YH5X.ConsultasC1.

29 Patent: Ramon Ferreiro Garcia. Gas turbine operating with baro-thermal pulses and operating procedure. Publication number: ES2851381 A1(06.09.2021), Also published as: ES2851381 B2 (27.07.2022). Applicant: FERREIRO GARCIA, Ramón (100.0%) (ES). IPC: *F02C3/02 (2006.01).* https://consultas2.oepm.es/InvenesWeb/faces/busquedaInternet.jsp;jsessionid=MDE3o-IscfQB7FbFuhlvN2mR.srvvarsovia1. https://consultas2.oepm.es/InvenesWeb/detalle?referencia=P202000032

30 V.Frolov, I.Matveev, D.Ivanov, S.Zverev, B.Ushin, G. Petrov, Experimental Investigation of the Hybrid Plasma Torch With Reverse Vortex Stabilization, January 2011 Romanian Journal of Physics 56. Retrieved 28-01-2026 from: https://www.researchgate.net/publication/268042256_Experimental_investigations_of_the_hybrid_plasma_torch_with_reverse_vortex_stabilization.

31 A Pascale T Lafleur and C S Corr, Parametric study of a vortex-enhanced supersonic inductive plasma torch. A Pascale *et al* 2024 *J. Phys. D: Appl. Phys.* **57** 435206. **DOI** 10.1088/1361-6463/ad687d

Retrieved on 28-01-2026 from:

https://translate.google.es/?langpair=en%7Ces&sl=en&tl=es&text=continuous%20high-flow%20quenching&op=translate

32 High-Power Electric Propulsion with VASIMIR Technology.
Retrieved from : https://www.unoosa.org/documents/pdf/psa/hsti/CostaRica2016/2-4.pdf.